An extension of the logistic function to account for nonstationary drought losses

Tongtiegang Zhao[1], Zecong Chen[1], Yongyong Zhang[2], Bingyao Zhang[3], and Yu Li[3]

[1] Southern Marine Science and Engineering Guangdong Laboratory (Zhuhai), School of Civil Engineering, Sun Yat-Sen University, Guangzhou 510275, China
[2] Key Laboratory of Water Cycle and Related Land Surface Processes, Institute of Geographic Sciences and Natural Resources Research, Chinese Academy of Sciences, Beijing 100101, China
[3] School of Hydraulic Engineering, Dalian University of Technology, Dalian 116024, Liaoning, China

Corresponding author: Tongtiegang Zhao (zhaottg@mail.sysu.edu.cn) and Zecong Chen (chenzc8@mail2.sysu.edu.cn)

带格式的：上标
带格式的：上标
带格式的：上标

Highlights:

1. The drought-affected population in mainland China exhibits ~~significant~~ remarkable correlation not only with standard precipitation index, but also with time;
2. The nonstationarity of drought losses is effectively characterized by incorporating time into the parameters of the classic logistic function;
3. The three nonstationary intensity loss functions built upon the logistic function are demonstrated to be a useful tool for drought impact assessment.

Abstract: While the intensity loss function based on stationary assumptions is fundamental to drought impact assessment, the relationship between drought loss and intensity can be nonstationary, i.e., changing as time progresses, owing to socio-economic developments. This paper addresses this critical gap by proposing a framework to model nonstationary drought losses. ~~builds three novel intensity loss functions upon the classic logistic function to account for nonstationary drought losses.~~ Specifically, the time is explicitly formulated as an explanatory variable and respectively incorporated into the magnitude, shape and location parameters of the logistic function to derive three nonstationary intensity loss functions. To examine the effectiveness, a case study is designed~~vised~~ for the drought-affected population by province in mainland China during the period from 2006 to 2023. The results highlight the existence of nonstationarity in that the drought-affected population exhibits significant correlation not only with standard precipitation index but also with year. The three nonstationary intensity loss functions are shown to outperform the classic logistic function and also the linear regression. They present effective characterizations of observed drought loss in different ways: 1) the nonstationary function with the flexible magnitude parameter fits the data by adjusting the maximum drought loss by year; 2) the nonstationary function with the flexible shape parameter works by modifying the growth rate of drought loss with intensity; and 3) the nonstationary function with the flexible location parameter acts by shifting the response curves along the axis by year. In general, the nonstationary function with the flexible magnitude parameter is shown to be the most promising in terms of high coefficient of determination, low Bayesian information criterion and explicit physical meaning. Taken together, the nonstationary intensity loss functions developed in this paper can serve as an effective tool for drought management.

Short summary: The classic logistic function characterizes the stationary relationship between drought loss and intensity. This paper incorporates the time into the three parameters of logistic function and derives three nonstationary intensity loss functions. The functions are tested through a case study of drought-affected population by province in mainland China during the period from 2006 to 2023. Overall, the nonstationary intensity loss functions are shown to be a useful tool for drought management.

1 Introduction

Droughts are one of the most destructive natural hazards (Baez-Villanueva et al., 2024; Van Dijk et al., 2013; Zhang et al., 2022). In general, there exist meteorological, hydrological, agricultural and socio-economic droughts (Mishra and Singh, 2010). Originating from precipitation deficits and high atmospheric evaporative demands, droughts propagate through hydrological processes and eventually impair human beings and natural ecosystems (Gao et al., 2024a; Liu et al., 2024; Zhao et al., 2024a). From 2001 to 2009, the "Millennium Drought" in Southeast Australia amplified median rainfall reduction by up to 4 times in streamflow and reduced irrigated rice and cotton production respectively by 99% and 84% (Van Dijk et al., 2013). The 2012 summertime drought arrived at the Central Great Plains in North America without early warning and caused more than US$30 billion of economic losses (Hoerling et al., 2014; Yuan et al., 2023). The 2021/22 drought event made 76.2% of the Euro-Mediterranean region under mild drought, 61.4% under moderate drought and 39.4% under severe drought (Garrido-Perez et al., 2024). Under climate change, droughts are expected to not only increase worldwide (Dai, 2011) but also intensify more rapidly (Yuan et al., 2023).

Socio-economic losses are an integral part of droughts in environment management (AghaKouchak et al., 2021; Hoerling et al., 2014; Van Dijk et al., 2013). Although there exist extensive studies on hydroclimatic processes relating to droughts (Entekhabi, 2023; Mishra and Singh, 2010; Wang et al., 2023b; Yang et al., 2024; Zhang et al., 2021), far less attention is paid to socio-economic impacts of droughts (AghaKouchak et al., 2021; Apurv and Cai, 2021; Su et al., 2018). One possible cause is the lack of socio-economic data on droughts (Su et al., 2018; Yang et al., 2024). On the one hand, ~~that~~ in situ observations, satellite remote sensing and earth system models generate a vast amount of hydroclimatic data (Hersbach et al., 2020; Pradhan et al., 2022; Zhang et al., 2024, 2021; Zhao et al., 2024b). Plenty of spatial-temporal data facilitate drought investigations at catchment, regional, continental and global scales and in pentad, monthly, seasonal and annual timesteps (Gao et al., 2024b; Ma et al., 2022; Wang et al., 2023a). On the other hand, there are limited data on drought-related socio-economic losses (AghaKouchak et al., 2021). Usually, drought losses have to be collected from statistical yearbooks issued by local and central governments and from survey reports provided by international organizations and commercial services (Chen et al., 2015; Hou et al., 2019).

The intensity loss function, which is also called exposure-response ~~function~~curve and dose–response relationship, plays a critical part in disaster risk management~~drought impact assessment~~ (AghaKouchak et al., 2021; Qiu et al., 2023; West et al., 2019). On the one hand, the classic logistic function is effective in characterizing the growth of socio-economic loss with drought intensity (Chen et al., 2015; Hou et al., 2019; Todisco et al., 2013). On the other hand, the relationship between socio-economic loss and drought intensity can be nonstationary, i.e., temporally changing, considering that economic growth can increase the exposure to droughts and that infrastructure developments can ~~decrease~~ increase the ~~vulnerability~~ resilience to droughts (Apurv and Cai, 2021; Haile et al., 2020; Long et al., 2020). In this paper, we build three non-stationary intensity loss functions upon the classic logistic function that represents a stationary intensity loss function. As will be illustrated in the

methods and results, the proposed functions tend to capture the non-stationary characteristics of drought-affected population in mainland China. The effects of drought intensity and time on population in different provinces are effectively characterized.

2 Methods

2.1 Intensity loss function

Drought indices are essential for drought impact assessment (Montanari et al., 2023; Todisco et al., 2013; West et al., 2019). Among the popular indices are the standardized precipitation index (SPI), the Palmer drought severity index (PDSI), the standardized precipitation evapotranspiration index (SPEI) and the standardized runoff index (SRI) (AghaKouchak et al., 2021; Apurv and Cai, 2021; Zhao et al., 2024b). The intensity is derived from drought indices (Hao et al., 2017; Mishra and Singh, 2010; Su et al., 2018). Since 0 is both the mean and median values of the standard normal distribution, the extent to which drought indices falling below 0 indicates the degree of dryness. Thresholds can be employed to identify drought events (Wang et al., 2023b). For example, (–0.99, 0] is near normal, (–1.49, –1.00] is moderately dry, (–1.99, –1.50] is severely dry and (–∞, –2.00] is extremely dry. Therefore, drought events can be defined by the combinations of multiple indices, e.g., by $SPI \leq -1.0$, $PDSI \leq -2.0$ and $SPEI \leq -1.0$ (Su et al., 2018).

Denoting the drought intensity as *I*, the intensity loss function is formulated as:

$$L = f(I) \tag{1}$$

带格式表格

in which *L* is the drought loss corresponding to the intensity *I*. Empirically, there are four important characteristics of $f(I)$: 1) there is minimal loss when there is minimal *I*; 2) there is maximal loss when there is maximal *I*; 3) $f(I)$ is a monotonically increasing function, i.e., drought loss increases with drought intensity; and 4) drought loss initially grows approximately exponentially with *I*, slows to linear as saturation begins and finally stops at maturity.

The above four characteristics can mathematically be formulated by the renowned logistic function (Chen et al., 2015; Jonkman et al., 2008; Kucharavy and De Guio, 2011):

$$L(I) = \frac{A}{1 + e^{-k(I-c)}} \tag{2}$$

带格式表格

in which there are three parameters: 1) the magnitude parameter *A* representing the maximum drought loss; 2) the shape parameter *k* controlling the growth rate of *L* with *I*; and 3) the location parameter *c* indicating the point at which the saturation begins.

As to drought indices that represent the intensity, they can be derived from the target hydroclimatic variable's cumulative distribution function (CDF) and the inverse CDF of the standard normal distribution (Hao et al., 2017; Mishra and Singh, 2010; Montanari et al., 2023; Zhang et al., 2024; Zhao et al., 2024b). For example, the SPI is calculated as:

$$SPI_t = CDF_{N(0,1)}^{-1}\left(CDF_p(p_t)\right) \quad (3)$$

in which SPI_t in period t, which follows the standard normal distribution, is derived from precipitation amount p_t in period t. There are two steps. Firstly, p_t is converted into a standard uniform variate between 0 and 1 by its CDF, i.e., $CDF_p(\cdot)$. Secondly, the standard uniform variate is converted into the standard normal variate SPI_t by the inverse CDF of $N(0,1^2)$, i.e., $CDF_{N(0,1)}^{-1}(\cdot)$. Similarly, ~~These additional indices are introduced to further investigate drought intensity and persistence, incorporating both precipitation and potential evapotranspiration (PET) in the analysis.~~

~~A similar methodology is applied in the calculation of~~the SPEI is derived from the difference between precipitation and potential evapotranspiration (Baez-Villanueva et al., 2024). Furthermore, the self-calibrating PDSI (scPDSI) takes into account eight variables, i.e., evapotranspiration, potential evapotranspiration, recharge, potential recharge, runoff, potential runoff, loss and potential loss, to report dry conditions with frequencies that would be expected for rare conditions (Wells et al., 2004).~~:~~

~~$$SPEI_t = CDF_{N(0,1)}^{-1}\left(CDF_p(p_t - PET_t)\right)$$~~

~~In which $SPEI_t$ is derived from the difference between precipitation amount p_t and the estimated potential evapotranspiration PET_t over a given period t.~~

~~In addition, the scPDSI is calculated as an self-calibrating version of the original PDSI, which normalizes drought severity over time:~~

~~$$scPDSI = K_t(X - X_{avg})$$~~

~~Where X is the observed hydroclimatic variable, X_{avg} is the long-term average of X. K_t is a calibration factor that adjusts the index to regional climate conditions(Wells et al., 2004).~~

2.2 Formulation of the logistic function

There is an inverse relationship between drought intensity and drought indices like SPI, ~~PDSI,~~ SPEI and scPDSI~~SRI~~. It is because the extent of dryness is generally characterized by how negative drought indices are (Haile et al., 2020; Liu et al., 2024; Zhang et al., 2021). That is, the more intensive dryness, the more negative drought indices. Taking the SPI as an indicator of drought intensity, the logistic function is modified by removing the negative sign in front of k:

$$L(SPI) = \frac{A}{1 + e^{k(SPI-c)}} \quad (4)$$

The ranges of the three parameters can be predetermined in accordance with the physical meanings of the parameters. First of all,

$$A > 0 \quad (5)$$

which means that drought loss is always above zero. Secondly,

带格式表格

带格式表格

带格式表格

带格式的: 字体: (中文) +中文正文 (宋体), (中文) 中文(中国)

带格式表格

带格式表格

$$k > 0 \tag{6}$$

which means that as *SPI* increases from $-\infty$ to $+\infty$, the denominator in Eq. (64) increases and leads to the reduction of drought loss. Eventually, the increasing denominator makes drought loss approach zero when SPI is large enough. On the other hand, it is noted that the loss would turn to increase with SPI when *k* is negative. Thirdly,

$$-\infty < c < +\infty \tag{7}$$

which means that the value of *c* depends on the case under investigation and can change freely.

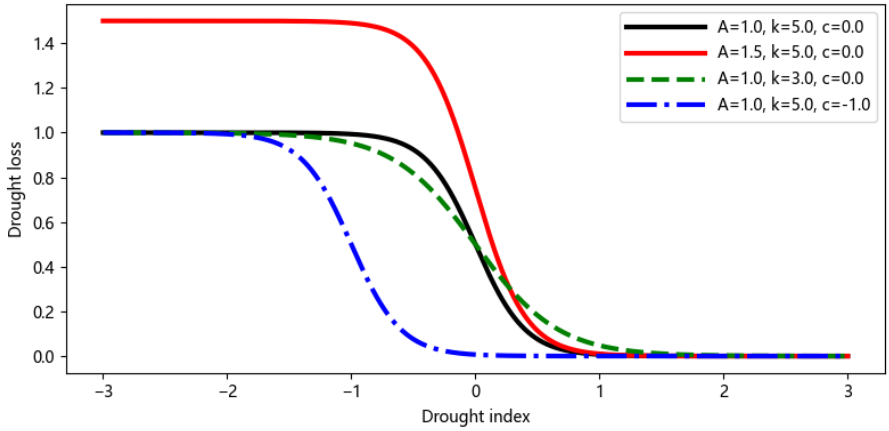

Figure 1. An illustrative example of the logistic function under four sets of parameters.

An illustrative example of the logistic function in Eq. (644) is presented in Figure 1. The result under the basic parameter set of (*A*=1.0, *k*=5.0, *c*=0.0) is marked in black. There are three one-factor-at-a-time experiments (Chen and Zhao, 2020). Firstly, the value of *A* is increased to 1.5. As is shown by the red line, the maximum drought loss evidently increases but the shape of the line stays the same. Secondly, the value of *k* is reduced to 3.0. As is shown by the green line, the shape of the line becomes flatter but the maximum loss remains the same. Thirdly, the value of *c* is decreased to –1.0. As is shown by the blue line, the plot is shifted to the left as a whole while both the maximum loss and shape do not change.

2.3 Stationary and non-stationary formulations

There are socio-economic factors contributing to temporal changes, i.e., nonstationarity, of the intensity loss function (AghaKouchak et al., 2021; Chiang et al., 2021; Long et al., 2020). Firstly, the ~~maximum drought loss~~exposure to drought can increase with time owing to increases of population ~~and,~~ accumulations of wealth and developments of infrasturture. Secondly, the vulnerability ~~loss~~ under a given level of drought intensity may decrease with time considering engineering measures, such as constructions of water storage reservoirs and inter-basin water diversion projects. Thirdly, the ~~growth rate of drought loss with drought intensity~~resilience to drought can be improved ~~attenuated~~ by ~~non-engineering~~ drought management measures such as subseasonal to seasonal hydroclimatic forecasting and forecast-informed reservoir operation. In general, the relationship between drought loss and intensity tends to evolve ~~is sophisticated~~ as time progresses due to ~~by~~ socio-economic developments and deployments of engineering and non-engineering drought-coping strategies~~and~~ (Hou et al., 2019; Jonkman et al., 2008; Su et al., 2018).

Without considering temporal changes~~the trend terms~~, there is a stationary logistic function $L_{A0k0c0}(\cdot)$:

$$L_{A0k0c0}(SPI_t) = \frac{A_0}{1 + e^{k_0(SPI_t - c_0)}} \tag{8}$$

To ~~In order to~~ account for temporal changes ~~(Cheng et al., 2014; Xiong et al., 2015),~~ , the linear function that takes time t as an explanatory variable (Cheng et al., 2014; Xiong et al., 2015) can be formulated for the parameters A, k and c:~~the time t is explicitly taken as an explanatory variable and then respectively incorporated into the parameters A, k and c (Cheng et al., 2014; Xiong et al., 2015):~~

$$\begin{cases} A_t = A_0 + A_1 \times t \\ k_t = k_0 + k_1 \times t \\ c_t = c_0 + c_1 \times t \end{cases} \tag{9}$$

带格式表格

in which A_0, k_0 and c_0 are the intercepts while A_1, k_1 and c_1 are the linear trends. ~~in which A_0, k_0 and c_0 are intercept terms while A_1, k_1 and c_1 are trend terms.~~The incorporation of Eq. (9) into Eq. (8) yield the following three equations: ~~Incorporating A_t into Eq. (69), the logistic function $L_{A1k0c0}(\cdot)$ with a nonstationary magnitude parameter is derived:~~

$$\begin{cases} L_{A1k0c0}(SPI_t) = \dfrac{A_0 + A_1 \times t}{1 + e^{k_0(SPI_t - c_0)}} \\ L_{A0k1c0}(SPI_t) = \dfrac{A_0}{1 + e^{(k_0 + k_1 \times t) \times (SPI_t - c_0)}} \\ L_{A0k0c1}(SPI_t) = \dfrac{A_0}{1 + e^{k_0(SPI_t - (c_0 + c_1 \times t))}} \end{cases} \tag{10}$$

in which the logistic functions $L_{A0k1c0}(\cdot)$, $L_{A0k1c0}(SPI_t)$ and $L_{A0k0c1}(SPI_t)$ respectively have nonstationary magnitude, shape and location parameters.

Furthermore, the quadratic function can be used to accommodate possible nonlinear changes:

$$\begin{cases} A_t = A_0 + A_1 \times t + A_2 \times t^2 \\ k_t = k_0 + k_1 \times t + k_2 \times t^2 \\ c_t = c_0 + c_1 \times t + c_2 \times t^2 \end{cases} \quad (11)$$

The incorporation of Eq. (11) into Eq. (8) yield another three equations:

~~$$L_{A1k0c0}(SPI_t) = \frac{A_0 + A_1 \times t}{1 + e^{k_0(SPI_t - c_0)}} \quad (10)$$~~

~~Incorporating k_t into Eq. (69), the logistic function $L_{A0k1c0}(\cdot)$ with a nonstationary shape parameter is derived:~~

~~$$L_{A0k1c0}(SPI_t) = \frac{A_0}{1 + e^{(k_0 + k_1 \times t) \times (SPI_t - c_0)}} \quad (11)$$~~

~~Incorporating c_t into Eq. (69), the logistic function $L_{A0k0c1}(\cdot)$ with a nonstationary location parameter is derived:~~

~~$$L_{A0k0c1}(SPI_t) = \frac{A_0}{1 + e^{k_0(SPI_t - (c_0 + c_1 \times t))}}$$~~

$$\begin{cases} L_{A2k0c0}(SPI_t) = \dfrac{A_0 + A_1 \times t + A_2 \times t^2}{1 + e^{k_0(SPI_t - c_0)}} \\ L_{A0k2c0}(SPI_t) = \dfrac{A_0}{1 + e^{(k_0 + k_1 \times t + k_2 \times t^2) \times (SPI_t - c_0)}} \\ L_{A0k0c2}(SPI_t) = \dfrac{A_0}{1 + e^{k_0(SPI_t - (c_0 + c_1 \times t + c_2 \times t^2))}} \end{cases} \quad (~~13~~12)$$

In Eq. (8), Eq~~s~~. (1~~2~~09) ~~to~~ and Eq. (14~~2~~2), the~~re are~~ subscripts "Ax", "kx" and "cx" are respectively for the magnitude, shape and location parameters. ~~for the intensity loss function.~~ As to "x", the values 0 ~~and,~~ 1 and 2 respectively indicate the non-involvement of time, the linear function of time and the quadratic function of time. As a result, the logistic function becomes non-stationary when x is 1 or 2. For example, $L_{A1k0c0}(SPI_t)$ represents the nonstationary logistic function involving the linear function of time for the magnitude parameter.

~~the non-use and use of time t. Accordingly, there is one stationary function $L_{A0k0c0}(\cdot)$ and three non-stationary functions $L_{A1k0c0}(\cdot)$, $L_{A0k1c0}(\cdot)$ and $L_{A0k0c1}(\cdot)$. The fitting of these functions is considered as a nonlinear least-squares problem by searching for the set of parameters that minimize the sum of squares of residuals. It is performed by the curve_fit function under the scipy optimization toolbox in Python (Virtanen et al., 2020).In order to investigate the potential nonlinear relationship, each function incorporates nonlinear trends in the following structure respectively in Eqs. (15):~~

The fitting of these functions is considered ~~as~~to be a nonlinear least-squares problem by searching for the set of parameters that minimize the sum of squares of residuals. It is performed by the curve_fit function under the ~~scipy~~SciPy optimization toolbox in Python (Virtanen et al., 2020).

3 Case study

3.1 Data description

~~To test the stationary and nonstationary intensity loss functions, t~~The drought loss data is sourced from the Ministry of Water Resources (MWR) of China to test the stationary and nonstationary intensity loss functions. It is noted that the MWR has since 2006 published by year "Bulletin of Flood and Drought Disaster in China". The name of the bulletin was changed to "China Flood and Drought Disaster Prevention Bulletin" in 2019. By collating floods and droughts reported by provincial governments and river basin commissions, the MWR has presented in the bulletin major events of droughts and floods across the 31 provinces in mainland China. As to droughts and floods in each province, the bulletin provides by year the quantitative socio-economic losses, contingency plans and retrospective analysis of prevention and control measures.

The attention is paid to the drought-affected population, which represents the actual number of individuals ~~impacted by~~suffering from drought events as recorded in official reports. In Figure 2 are the multi-annual mean drought-affected population, maximum annual drought-affected population, mean annual precipitation and total population. From Figures 2a and 2b, it can be observed that provinces in Southwest China, including Yunnan, Guizhou and Sichuan Provinces, tend to have the largest ~~drought-affected~~ population suffering from drought. Particularly in 2010, 8.82 million people in Yunnan Province and 5.44 million people in Guizhou Province were struck by a record-breaking drought event induced by the persistently positive Madden-Julian Oscillation (Lü et al., 2012). On the other hand, it can be seen from Figures 2c and 2d that there is neither low precipitation nor large population in Southwest China. In general, the large drought-affected population in Yunnan and Sichuan Provinces is attributed to the Karst landscape, which features small storage capacity, high infiltration rate and fast groundwater flow (Wan et al., 2016).

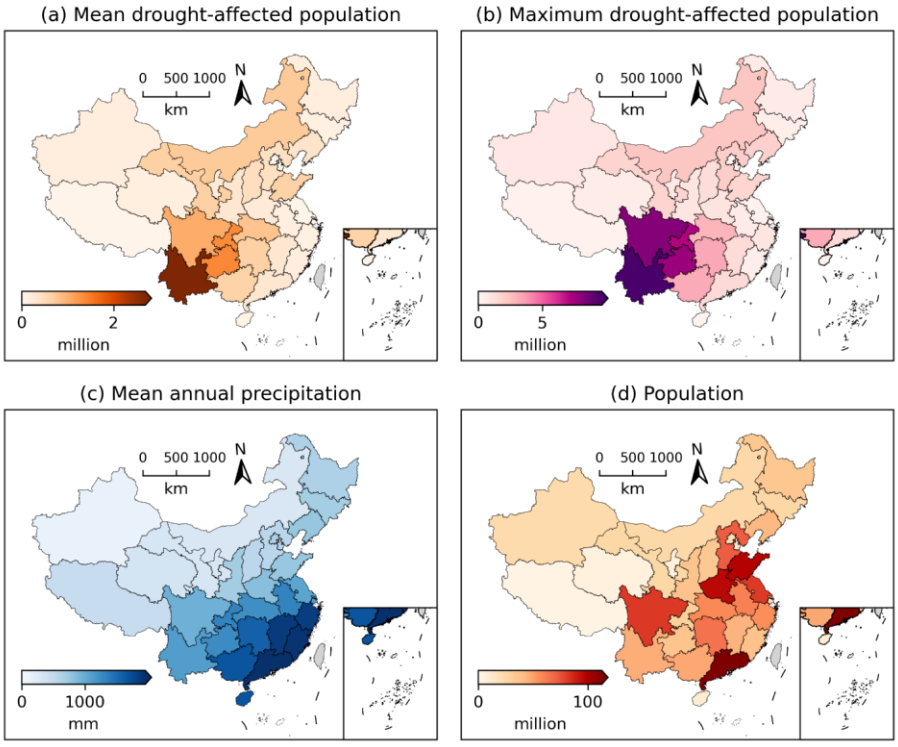

Figure 2. Spatial plots of (a) mean annual drought-affected population, (b) maximum annual drought-affected population, (c) mean annual precipitation and (d) population by province in mainland China.

The precipitation data used for the calculation of SPI is obtained from the Climate Hazards Group InfraRed Precipitation with Station data (CHIRPS) (Funk et al., 2015). The intersection operation is performed to use provincial polygons to extract spatially averaged precipitation from the raster CHIRPS precipitation field. To better characterize the climatological distribution of precipitation, time series of annual precipitation are extracted by province for the period from 1981 to 2023. The 43 years' annual precipitation is firstly converted into CDF by the Weibull's plotting position (Ye et al., 2018) and then converted into SPI by the inverse CDF of $N(0,1^2)$. Then, the SPI in the years from 2006 to 2023 is used in the fitting of the logistic functions.

Alongside the SPI, Tthe SPEI data is obtained from the SPEIbase v.2.10 SPEIbase the Cliamtic Research Unit version 2.10 (Beguería et al., 2024). Specifically, the time scales is 12 months and the SPEI-12 in December is selected to represent the annual drought condition as the loss is at the timescale of 12 months; and the intersection operation is performed to use provincial polygons to extract spatially averaged SPEI. Furthermore, the scPDSI is sourced from the the Climate Research Unit (CRU) (Barichivich et al., 2024) SPEIbase v.2.10 (Beguería et al., 2024). As this dataset provides monthly scPDSI, the values across the 12 months are averaged before calculating the spatially averaged SPEI.

. Then, the intersection operation is performed to use provincial polygons to extra spatially averaged SPEI. The provincial annual scPDSI is calculated by averaging the monthly scPDSI calculated using CRU TS (Barichivich et al., 2024; van der Schrier et al., 2013) for each year and extracted by province(van der Schrier et al., 2013).

3.2 Model evaluation

The coefficient of determination, i.e., R^2, is evaluated for the stationary logistic function (Eq. 98) and the three six types of nonstationary logistic functions (Eqs. 10, 11 and 12). That is, the sum of squares of residuals for the estimations provided by the functions is compared to the baseline sum of squares of residuals for the mean value. As a result, R^2 represents the ratio of total variation of the drought loss that is explained:

$$R^2 = 1 - \frac{\sum_t (L_t - \hat{L}_t)^2}{\sum_t (L_t - \bar{L})^2} \quad (14)(13)$$

带格式表格

in which L_t is the drought loss in year t, $\hat{L}_t$ is the loss estimated by the function under investigation and $\bar{L}$ is the mean value of all L_t.

The number of parameters plays a critical part in statistical modelling. That is, more parameters facilitate more flexible fitting of observed data but in the meantime, are more prone to overfitting (Neath and Cavanaugh, 2012). There are 3 parameters for the stationary logistic function, 4 parameters for the non-stationary logistic functions with the linear function and 5 parameters for the non-stationary logistic functions with the quadratic function:respectively 3 and 4 parameters in the stationary and nonstationary logistic functions, and 5 parameters in the nonstationary logistic function incorporating a quadratic term:

$$\begin{cases} n_{A0k0c0} = 3 \\ n_{A1k0c0} = 4 \\ n_{A0k1c1} = 4 \\ n_{A0k0c1} = 4 \\ n_{A2k0c0} = 5 \\ n_{A0k2c0} = 5 \\ n_{A0k0c2} = 5 \end{cases} \quad (15)(14)$$

带格式表格

The Bayesian information criterion (BIC) takes into account both the sum of squares of residuals and the number of parameters (Neath and Cavanaugh, 2012):

$$BIC = T \times \ln\left(\frac{\sum_t \left(L_t - \hat{L}_t\right)^2}{T}\right) + n \times \ln(T) \quad (16)(15)$$

in which $\ln(\cdot)$ is the natural logarithmic function, T is the number of observations and n is the number of parameters. BIC is negatively oriented, meaning that a lower value indicates a better fit. As a result, both larger sum of squares of residuals and more parameters are penalized by the BIC.

带格式表格

4 Results

4.1 Correlation analysis

~~4.1 Correlation analysis~~

The Pearson's correlation coefficient between drought-affected population and time as well as SPI are illustrated by bar plots in Figure 3. There are in total 31 provincial administrative regions in mainland China. Beijing, Tianjin, Shanghai and Xizang are not considered since they are free from drought-affected population in most years. This outcome is mainly due to ample water supply by urban facilities ~~infrastructure developments~~ (Long et al., 2020; Sun et al., 2021). For the other 27 provincial administrative regions, it can be observed that the correlation coefficient between drought-affected population and time~~SPI~~ is mostly significantly negative except for Guangdong and Fujian Provinces. ~~A significance analysis indicates that most of the negative correlations between drought-affected population and time are statistically significant at the 0.01 or 0.05 level.~~ The implication is that the drought-affected population mostly exhibits a decreasing trend as time progresses and sometimes shows an increasing trend. In the meantime, the correlation coefficient between drought-affected population and SPI is in general significantly negative. ~~Similarly, for the correlation between drought-affected population and SPI, the majority of the negative correlations are statistically significant at the 0.1 or 0.05 level.~~ This result suggests that drought-affected population tends to decrease as the amount of precipitation increases. Overall, the correlation coefficients in Figure 3 point out that it is reasonable to use both time and SPI as explanatory variables of drought-affected population.

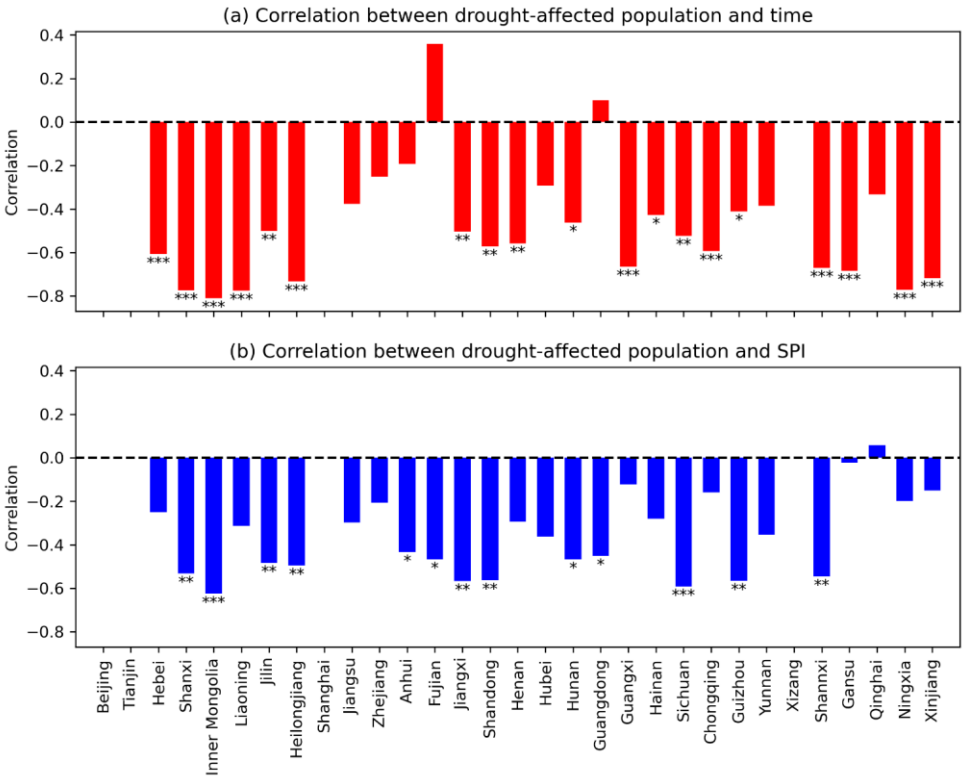
(a) Correlation between drought-affected population and time
Correlation
0.4
0.2
0.0
−0.2
−0.4
−0.6
−0.8
(b) Correlation between drought-affected population and SPI
Correlation
0.4
0.2
0.0
−0.2
−0.4
−0.6
−0.8
Beijing
Tianjin
Hebei
Shanxi
Inner Mongolia
Liaoning
Jilin
Heilongjiang
Shanghai
Jiangsu
Zhejiang
Anhui
Fujian
Jiangxi
Shandong
Henan
Hubei
Hunan
Guangdong
Guangxi
Hainan
Sichuan
Chongqing
Guizhou
Yunnan
Xizang
Shannxi
Gansu
Qinghai
Ningxia
Xinjiang

260

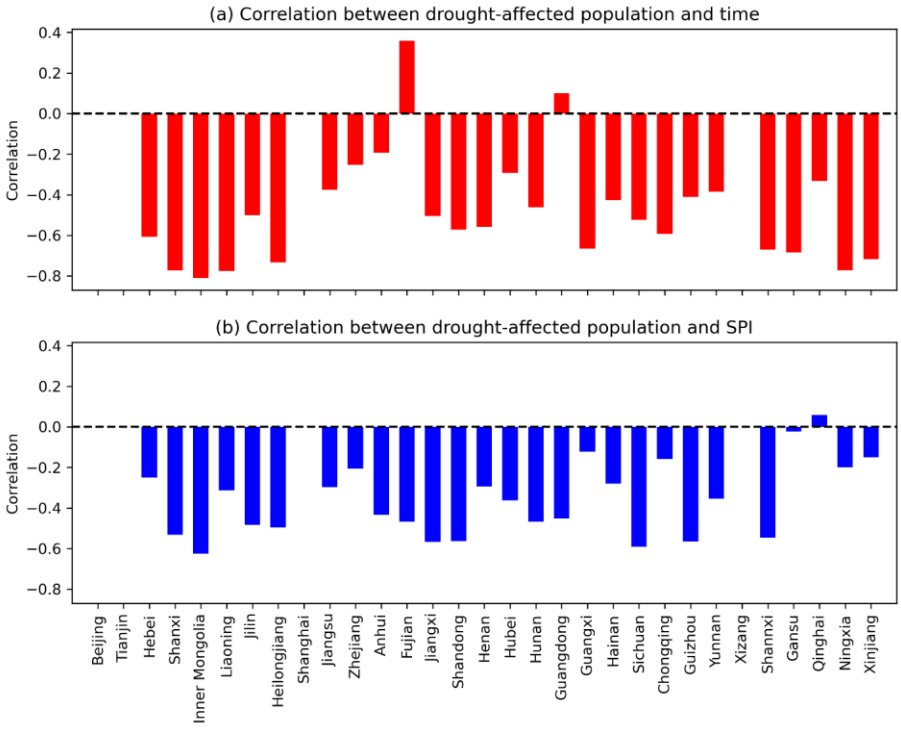

Figure 3. Correlation coefficient between drought-affected population and (a) time as well as (b) SPI by province. Alongside the bars are ~~,* indicate the significance level of the correlation,~~ *, ** and *** respectively indicating the significance at the levels of 0.10, 0.05 and 0.01. Bars without * imply non-significant correlation coefficients.

~~where p < 0.1 is marked by one star (*), p < 0.05 by two stars (**), and p < 0.01 by three stars (***)~~

带格式的: 字体: (中文) 宋体, (中文) 中文(中国)

带格式的: 默认段落字体, 字体: (中文) 宋体, (中文) 中文(中国)

带格式的: 默认段落字体, 字体: (中文) 宋体, (中文) 中文(中国)

The drought-affected population is plotted against time and SPI for Yunnan Province in Figure 4 and for Guangdong Province in Figure 5. The scatter plots on the left-hand side of the two figures imply the complexity of drought impact assessment. That is, owing to socio-economic developments, the drought-affected population can decrease or increase as time progresses (Apurv and Cai, 2021; Haile et al., 2020; Long et al., 2020). In the meantime, the scatter plots on the right-hand side suggest that the increase of precipitation amounts effectively reduces the population subject to droughts (AghaKouchak et al., 2021; Qiu et al., 2023; West et al., 2019).

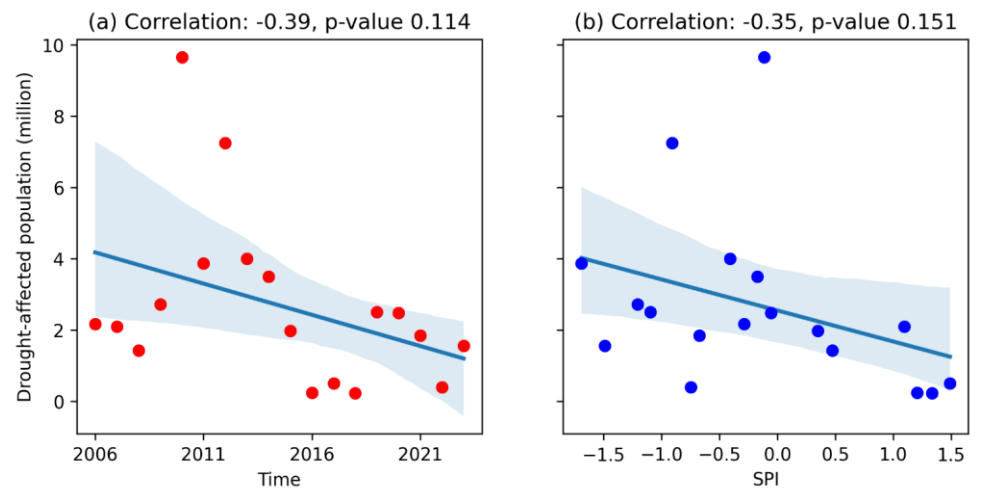
(a) Correlation: -0.39, p-value 0.114
(b) Correlation: -0.35, p-value 0.151
Drought-affected population (million)
Time
SPI

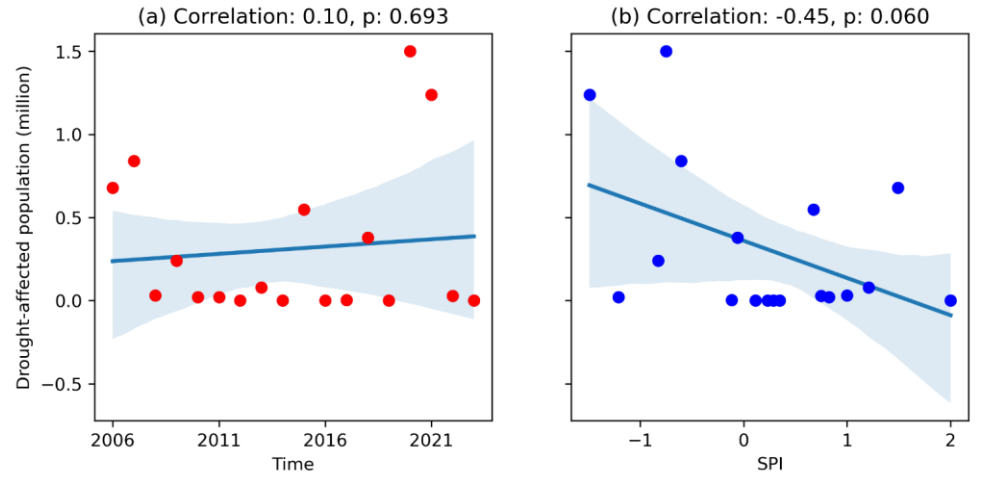
(a) Correlation: 0.10, p: 0.693
(b) Correlation: -0.45, p: 0.060
Drought-affected population (million)
Time
SPI

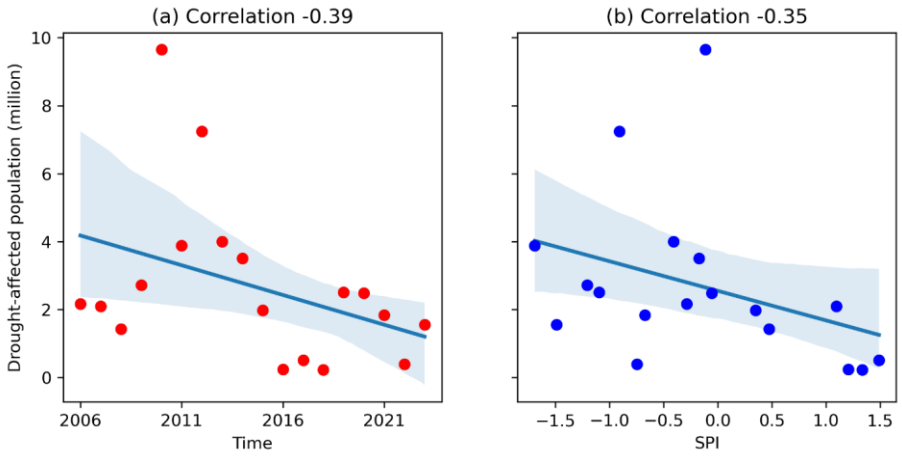

Figure 4. Scatter plots of drought-affected population against (a) time and (b) SPI in Yunnan Province.

带格式的：题注

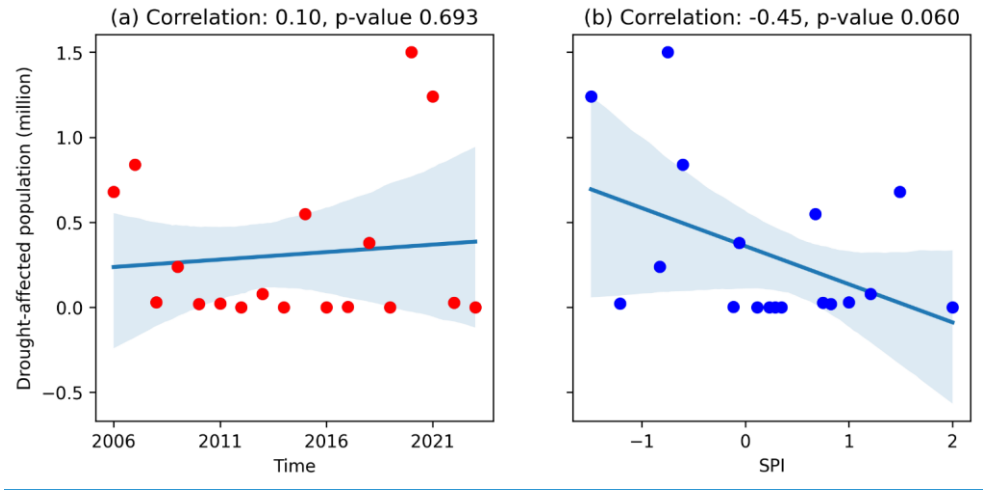
(a) Correlation: 0.10, p-value 0.693
(b) Correlation: -0.45, p-value 0.060
Drought-affected population (million)
Time
SPI

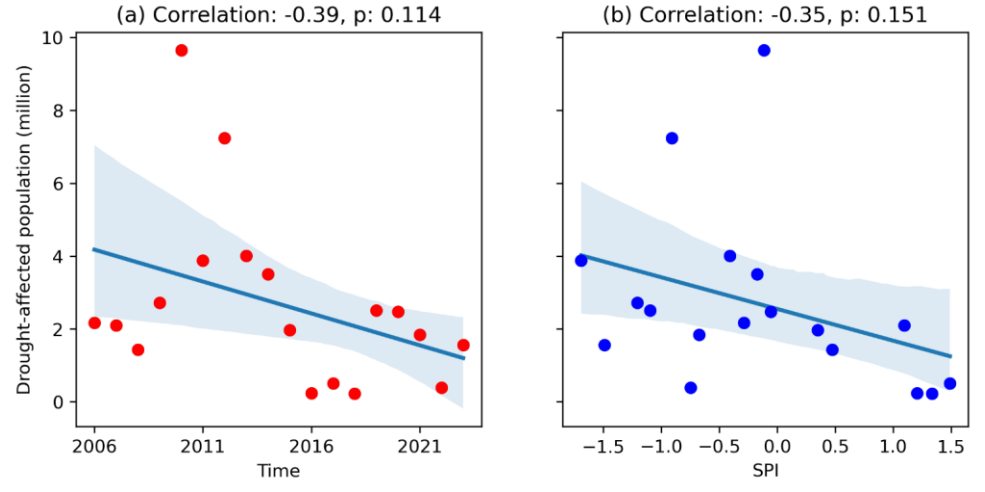
(a) Correlation: -0.39, p: 0.114
(b) Correlation: -0.35, p: 0.151
Drought-affected population (million)
Time
SPI

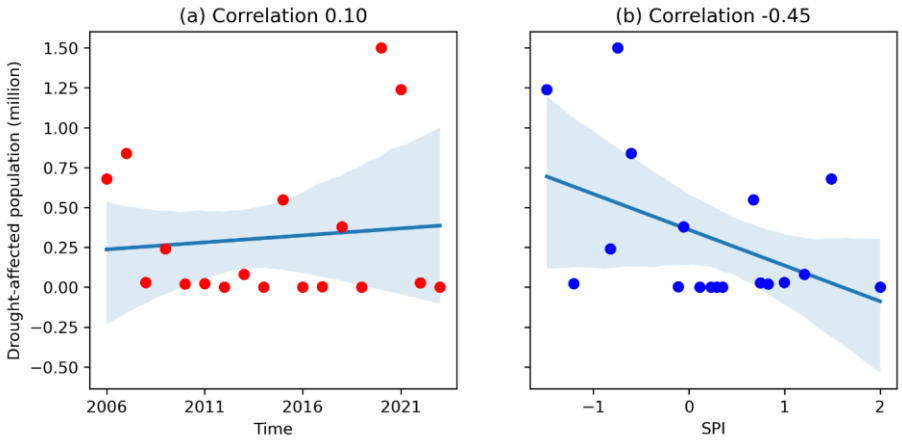

Figure 5. As for Figure 4, but for Guangdong Province.

4.2 Decreasing drought-affected population

The three nonstationary logistic functions are one-by-one fitted by relating the drought-affected population to time and SPI for Yunnan Province. The results are visualized by the surface and wireframe plots in Figure 6. The 3d scatter points suggest that the drought-affected population tends to decrease with SPI and that it exhibits a decreasing trend as time progresses from 2006 to 2023. The three nonstationary logistic functions are shown to be effective in generating 3d response surfaces to characterize the dependency relationships, with reasonable R^2 and BIC values. Meanwhile, they perform differently in capturing the observed data:

1) The flexible magnitude parameter in A1k0c0 tends to fit the observed data by reducing the maximum drought loss by year, as shown in Figure 64a. As can be seen from the wireframe plot, the maximum drought loss evidently reduces from 2006 to 2023 while the shape and location of the curves remain the same.
2) The flexible shape parameter in A0k1c0 fits the observed data by changing the response surface, as shown in Figure 64b. Although it exhibits the highest R^2 and the lowest BIC, the fitted drought-affected population is shown to counterintuitively increase with SPI in 2021, 2022 and 2023. That is, more people could be subject to drought as precipitation increases in these three years. This wrong outcome is owing to the flexibility of the shape parameter. Specifically, the value of the shape parameter can be forced by the trend term to turn from positive to negative as time progresses. When the shape parameter is negative, the estimated drought impact would increase with the precipitation amount.

3) The flexible location parameter in A0k0c1 tends to fit the observation data by shifting the response curves by year, as shown in Figure 64c. Due to that the maximum drought-affected population is fixed from 2006 to 2023, it is observed that the maximum affected population in 2010 is not effectively captured.

~~3)~~

305

带格式的: 题注, 无项目符号或编号

带格式的: 字体: (中文) +中文正文 (宋体), (中文) 中文(中国)

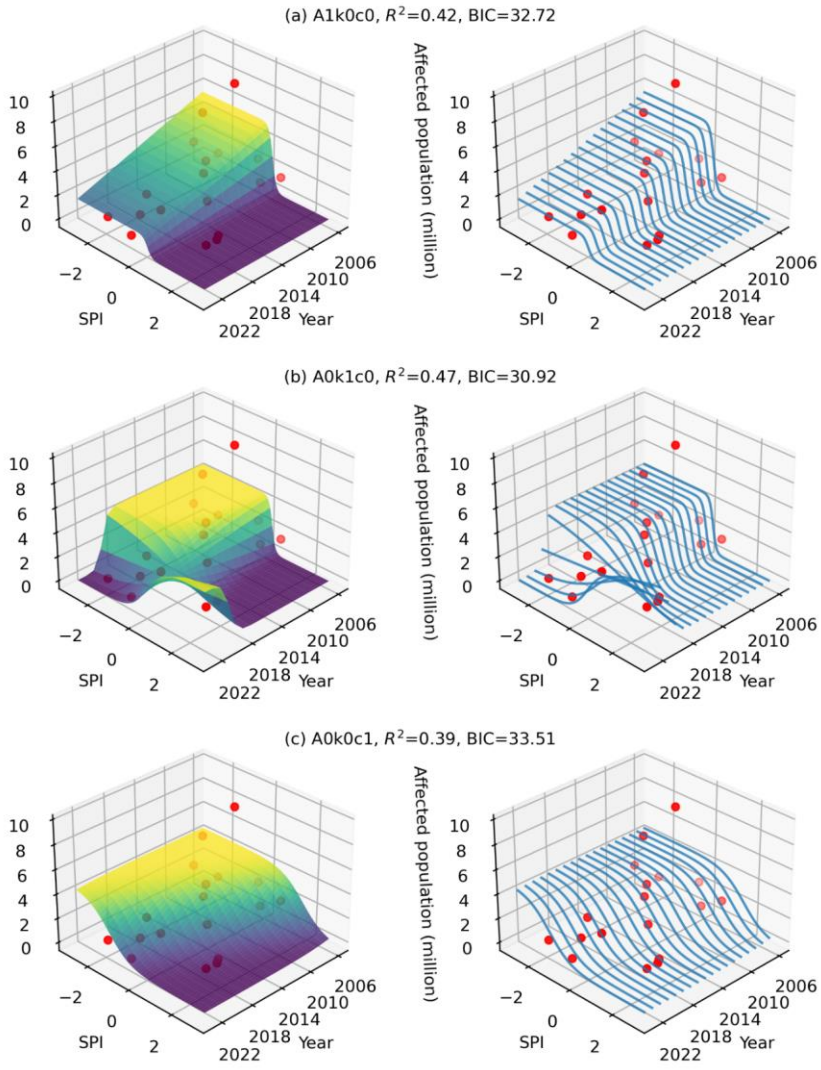

Figure 6. Surface plots (left) and wireframe plots (right) for the nonstationary logistic functions (a) A1k0c0, (b) A0k1c0 and (c) A0k0c1 relating the drought-affected population to time and SPI for Yunnan Province.

The fitted curve of baseline stationary function A0k0c0 in Yunnan(Fig 7) indicates a maximum drought-affected population of 3.75 millions, despite the largest observed affected population being 10 million. This discrepancy suggests that the model may underestimate the drought-affected population. When the SPI is larger than 0, the drought-affected population decreasing gradually as SPI increases beyond 0.

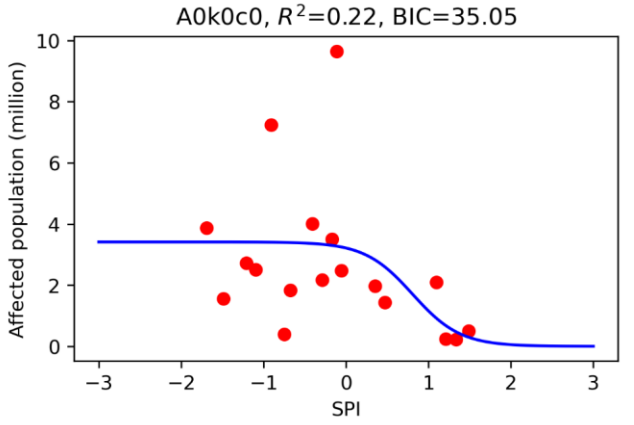

Figure 7. Fitting diagram ~~Curve plots~~ for the logistic functions A0k0c0 ~~relating the drought-affected population to SPI~~ for Yunnan Province.

4.3 Increasing drought-affected population

Given the importance of the Guangdong-Hong Kong-Macao Greater Bay Area (Shao et al., 2020), the dependency of drought-affected population on time and SPI in Guangdong Province is illustrated by the surface and wireframe plots in Figure 8~~7~~. Since the population of Guangdong is concentrated on the Pearl River Delta, recent years have witnessed serious water scarcity due to upstream reservoir impoundments and estuary saltwater intrusion (Weng et al., 2024). From Figure 8~~7~~, it can be observed that the three non-stationary logistic functions characterize the increasing drought-affected population in different ways:

带格式的: 正文

带格式的: 正文

带格式的: 题注

1) The flexible magnitude parameter in A1k0c0 tends to fit the increase by enlarging the maximum drought loss by year. As shown in Figure 8~~7~~a, it tends to capture the maximum drought-affected population of 1.50 million in 2020 and the second maximum drought-affected population of 1.24 million in 2021.

~~2)~~ The flexible shape parameter in A0k1c0 is observed to fit the observation data by changing the shape of response surface by year. As shown in Figure 8~~7~~b, although the affected population in 2020 and 2021 is to some extent characterized, drought-affected population is seen to surprisingly increase with SPI in 2006. These results highlight the role that the shape parameter plays in determining the growth (reduction) rate.

2)

~~3)~~ The flexible location parameter in A0k0c1 is shown to fit the observation data by fixing the maximum drought loss but shifting the response curves by year. As shown in Figure 8~~7~~c, it tends to characterize the maximum and second maximum drought-affected population in recent years but does not seem to be as effective in characterizing drought-affected population in early years.

3)

带格式的：字体: (中文) Times New Roman

带格式的：无项目符号或编号

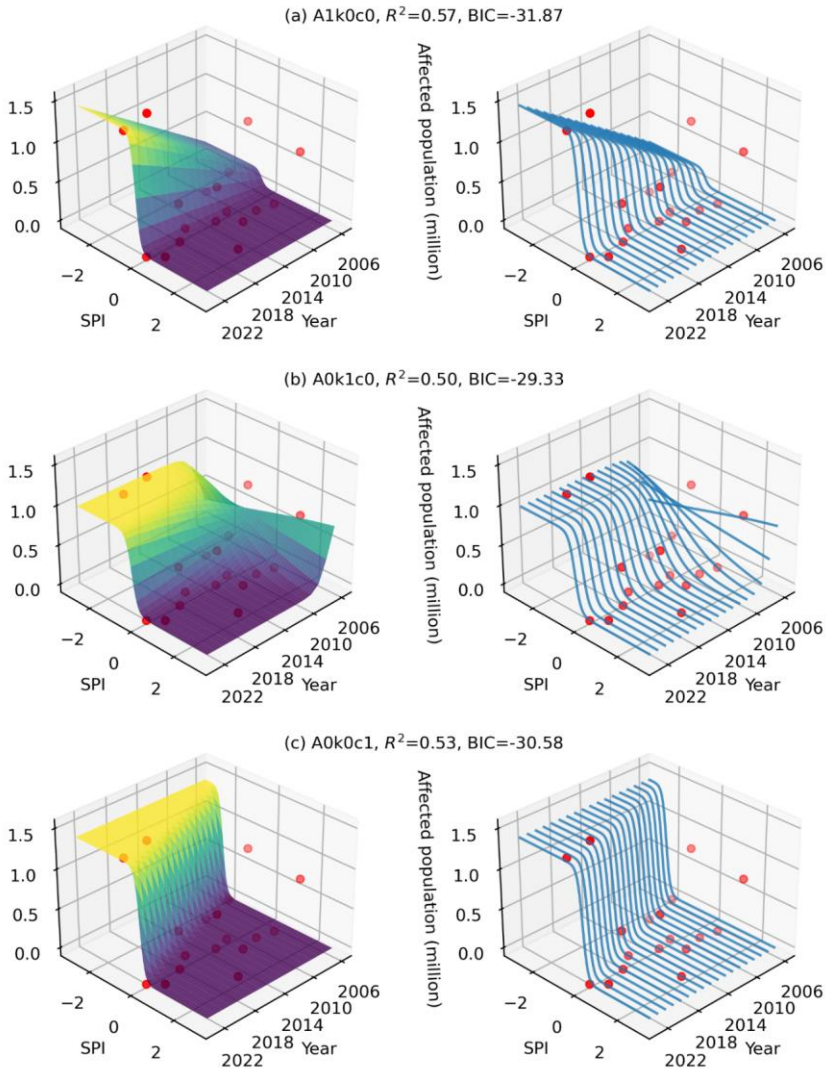

Figure 87. As for Figure 6, but for Guangdong Province.

The fitted curve of baseline stationary function A0k0c0 in Guangdong (Fig 9) indicates a maximum drought-affected population of 0.75 million. And the drought-affected population decreasing rapidly as SPI increases beyond -0.5.

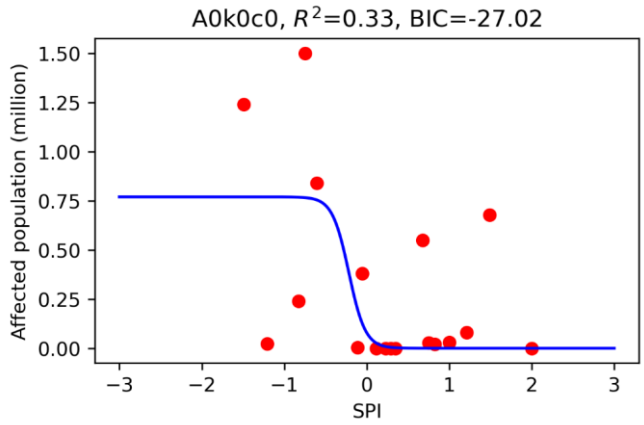

Figure 9. As for Figure 7, but for Guangdong Province.

4.4 Goodness-of-fit

The stationary and nonstationary logistic functions are set up to account for the drought-affected population based on the explanatory variables of time and SPI for 27 provincial administrative regions other than Beijing, Tianjin, Shanghai and Xizang. The R^2 for the three nonstationary logistic functions are plotted against that of linear regression based on time (Figure 10a) and also against that of the stationary logistic function (Figure 10b). The three scatter plots are generally above the 1:1 line. This result indicates that the consideration of time t evidently enhances the proportion of total variation explained by the non-stationary logistic functions. It is noted that the mean R^2 is respectively 0.307 for linear regression and 0.269 for the stationary logistic function A0k0c0. By contrast, the mean R^2 is respectively 0.512, 0.506 and 0.509 for A1k0c0, A0k1c0 and A0k0c1. Overall, the nonstationary logistic function A1k0c0 is of the highest R^2. This result highlights that the incorporation of time into the magnitude parameter can effectively deal with the non-stationary drought-affected population.

带格式的: 字体: 非加粗
带格式的: 字体: 非加粗
带格式的: 与下段不同页
带格式的: 字体: 非加粗
带格式的: 字体: 非加粗
带格式的: 字体: 非加粗
带格式的: 字体: 非加粗
带格式的: 字体: (中文) 宋体, (中文) 中文(中国)
带格式的: 居中, 与下段不同页
带格式的: 正文

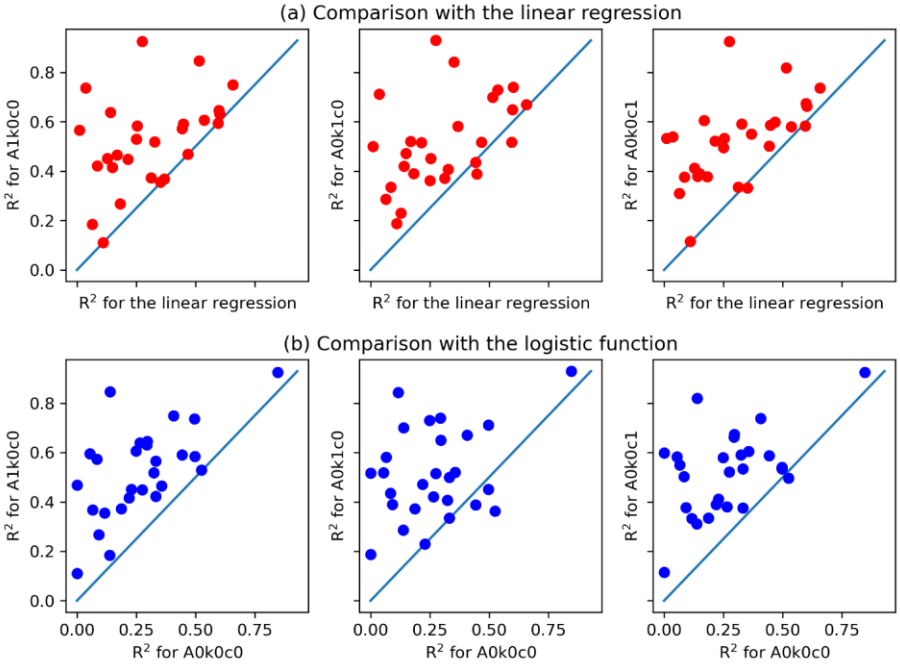

Figure 108. Scatter plots of the R^2 for the three nonstationary logistic functions against the R^2 for (a) the linear regression and (b) the stationary logistic function A0k0c0.

Furthermore, the BIC of the three nonstationary logistic functions is plotted against the BIC of the linear regression in Figure 119a and against that of the stationary logistic function in Figure 119b. Since the higher R^2 of the nonstationary logistic functions in Figure 118 is at the cost of an additional parameter (Neath and Cavanaugh, 2012), the BIC takes into account not only the number of parameters but also the mean squared error. It can be observed that the scatter plots in Figure 115 are largely below the 1:1 line. Considering that the BIC is a negatively oriented metric, this result suggests that there is a low risk of overfitting and that the information hidden in the significant correlation (Figure 3) is deemed to be effectively exploited by the three non-stationary logistic functions. It is noted that the mean BIC is respectively –33.105 for linear regression and –29.365 for the stationary logistic function A0k0c0. By contrast, the mean BIC is respectively –34.980, –34.772 and –34.740 for A1k0c0, A0k1c0 and A0k0c1. As the nonstationary logistic function A1k0c0 is of the lowest BIC, it is highlighted that the

incorporation of time into the magnitude parameter of the logistic function is effective in accounting for the non-stationarity of drought losses.

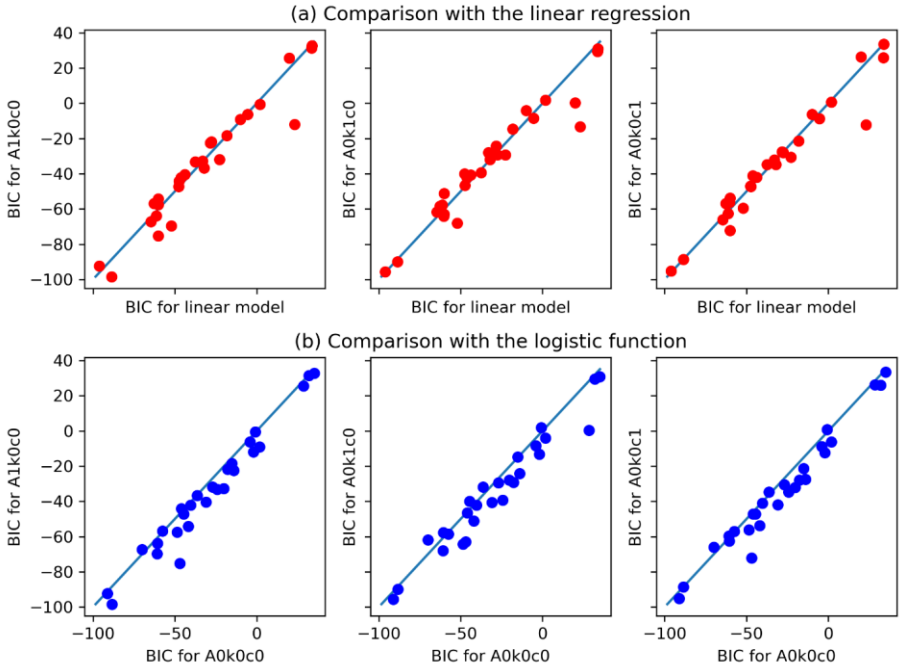

Figure 119. As for Figure 108, but for the BIC.

5 5 Discussion

5.1 Robustness analysis of nonstationary logistic functions

This paper has furthermore designed experiments to investigate the robustness of the nonstationary logistic functions using different drought indices such as SPEI and scPDSI. Specifically, the case studies in Figs.6 and 8 are performed using the SPEI

带格式的: 题注
带格式的: 字体: (中文) +中文正文 (宋体), (中文) 中文(中国)
带格式的: 正文
带格式的: 题注
带格式的: 多级符号 + 级别: 1 + 编号样式: 1, 2, 3, … + 起始编号: 4 + 对齐方式: 左侧 + 对齐位置: 0 厘米 + 缩进位置: 0.63 厘米
带格式的: 字体: (默认) Times New Roman, (中文) Times New Roman
带格式的: 字体: (默认) Times New Roman, (中文) Times New Roman
带格式的: 字体: (默认) Times New Roman, (中文) Times New Roman
带格式的: 列出段落, 多级符号 + 级别: 1 + 编号样式: 1, 2, 3, … + 起始编号: 4 + 对齐方式: 左侧 + 对齐位置: 0 厘米 + 缩进位置: 0.63 厘米

and scPDSI. The results of other two indices are found to have similar trend and are thus presented as supplementary material. ~~The Surface plots and wireframe plots of the SPEI (Appendix A) and scPDSI (Appendix B) for Yunnan and Guangdong Province are presented in the supplementary material.~~ In Figures S1~~A1~~, the surface plot of A0k1c0 for Yunnan Province fitted using SPEI differs from that fitted using SPI, the drought-affected populations decrease with SPEI in 2021 to 2023 due to the changes of the ~~extreme~~ low drought-affected populations and low SPI in the recsent year. In Figure S2, the surface plot of SPEI is similar to that of SPI for Guangdong Province. In Figures S3 and S4, the surface plots of scPDSI for Yunnan and Guangdong are presented, showing similarities to SPI-based plots for Guangdong province but appearing slightly smoother than those in Yunnan province.~~In Figure B1 and B2, the surface plot of Yunnan and Guangdong for scPDSI. The surface plots are similar as the SPI in Guangdong Province, and a little bit smoother than that in Yunnan Province.~~

To explore potential nonlinearity, this paper also incorporated a quadratic term of time into each form of nonstationary functions separately. In Yunnan Province (Fig. S5~~Appendix Figure C1~~), ~~the response surface for A0k0c2 shows a pattern similar to that of A0k0c1, maintaining a consistent structure. However,~~ significant~~notable~~ differences are observed when comparing A2k0c0 to A1k0c0, and A0k2c0 to A0k1c0. Specifically, the surface plot of A2k0c0 shows a parabolic pattern in maximum drought loss by year, while A1k0c0 fits the observed data by reducing the maximum drought loss over time. The surface plot of A0k2c0 shows an increasing trend in the estimated affected population with SPI in earlier years. This wrong outcome is caused by the same issue observed in A0k1c0, emphasizing the influence of the shape parameter's flexibility.~~Specifically, the A2k0c0 surface exhibits a parabolic shape, effectively capturing the maximum drought loss as a function of SPI and year. In contrast, the A0k2c0 surface indicates an increasing trend in the estimated affected population with SPI during earlier years, highlighting the model's sensitivity to the drought index.~~ In Guangdong Province (Fig. S6~~Appendix Figure C2~~), differences are observed when comparing A2k0c0 to A1k0c0, and A0k2c0 to A0k1c0 ~~the behavior of A0k2c0 closely resembles that of A0k1c0, with similar trends in the response surface~~. The~~For~~ surface plot of A2k0c0 ~~, the inclusion of a quadratic time term~~ transforms the trend of maximum drought loss from a linear increase in A1k0c0 to a concave quadratic curve, ~~effectively~~ capturing ~~temporal variations with~~ the lowest drought impact occurring in 2014. The surface plot of ~~In contrast,~~ A0k0c2 incorporates the quadratic term into the location parameter. This adjustment leads to a distinct shift in the response curve over time, resulting in a quadratic shifting trajectory.~~, resulting in a distinct shift in the response curve over time, forming a quadratic trajectory.~~

5.2 Applications and future research

The nonstationary intensity loss functions developed in this paper complement existing studies on hydroclimatic processes of droughts (Garrido-Perez et al., 2024; Haile et al., 2020; Todisco et al., 2013). Focusing on drought indices such as SPI, PDSI, SPEI and SRI, previous studies have presented in-depth investigations about past changes and future projections of

带格式的: 字体颜色: 自动设置
带格式的: 字体颜色: 自动设置
带格式的: 字体颜色: 自动设置
带格式的: 字体颜色: 自动设置
带格式的: 字体颜色: 自动设置
带格式的: 字体颜色: 自动设置
带格式的: 字体颜色: 自动设置
带格式的: 字体颜色: 自动设置
带格式的: 字体颜色: 深红

meteorological, hydrological, agricultural and socio-economic droughts (Apurv and Cai, 2021; Hao and Singh, 2015; Mishra and Singh, 2010). One remarkable feature of the proposed intensity loss function is the explicit estimation of drought loss under different combinations of SPI and time. In future studies, the relationship between drought loss and other drought indices can readily be investigated at local and regional scales. Given that the logistic function is already an established growth model in biosciences (Tsoularis and Wallace, 2002), it is expected that the proposed functions can be used to characterize the growth of drought loss with drought conditions characterized by different drought indices. ~~(Yin et al., 2022)(Gao et al., 2024c)(Shi et al., 2021)(Wu et al., 2006)More case studies are in demand to test the usefulness.~~

The frequency, duration and intensity are three important characteristics of drought (Baez-Villanueva et al., 2024; Entekhabi, 2023; Liu et al., 2024; Mishra and Singh, 2010; Yang et al., 2024). Given a threshold for the identification of drought events, the frequency is generally defined as the number of drought events in a certain period (one year for example), the duration as the timespan of a drought event and the intensity as the cumulative sum of the drought index (AghaKouchak et al., 2021; Chiang et al., 2021). Given that the SPI is derived for annual precipitation in this paper, the SPI values are expected to reflect the conditions of drought frequency, duration and intensity across different years. It is noted that the use of annual precipitation is mainly due to the fact that the drought-affected population by province is available at the annual timescale. It is possible that drought losses are available on an event scale. In that case, event-based analysis becomes feasible. That is, both drought loss and intensity can be quantified for each drought event; and then the effectiveness of the logistic function can be tested.

Droughts are increasingly found to be interconnected with other extreme events, leading to compound disasters, such as heatwaves (Yin et al., 2022), tropical cyclones (Gao et al., 2024c), drought-flood abrupt alternation (Shi et al., 2021) and summer drought-flood coexistence (Wu et al., 2006). As the frequency and intensity of these compound disasters continue to increase, the potential for drought losses is expected to rise. Additionally, socio-economic development may increase exposure to drought, thereby exacerbating the magnitude of drought-induced impacts. In this study, we use time as a covariate to capture the overall trend of nonstationary drought losses mentioned above. A significant correlation between drought losses and time has been observed in many provinces, as highlighted in our results. However, more case studies are needed to evaluate the nonstationarity induced by compound disasters and of social-economic growth.

6 Conclusions

This paper has presented three ~~novel~~ nonstationary intensity loss functions for drought impact assessment. On the one hand, the classic logistic function that has three parameters, i.e., magnitude, shape and location, presents a stationary formulation of the growth of drought losses with drought conditions. On the other hand, the incorporations of time respectively into the magnitude, shape and location parameters facilitate three nonstationary logistic functions. A case study is presented for the drought-affected population by province in China during the period from 2006 to 2023. The results highlight that despite the fact that drought-affected population can either decrease or increase with time, the joint use of both time and SPI as explainable variables leads to effective characterization of drought-affected population. In comparison with the stationary logistic function,

the effectiveness of the nonstationary logistic functions is indicated not only by higher R^2, which indicates reasonable proportion of total explained variation, but also by lower BIC, which suggests low risk of overfitting. Among the three nonstationary logistic functions, the function with nonstationary magnitude parameter generally outperform the other two in terms of higher R^2, lower BIC and clearer physical meanings. In conclusion, the nonstationary intensity loss functions developed in this paper can improve our understanding and respond to drought risks in an era of rapid socio-economic and environmental change. Future research could further enhance this framework by incorporating additional socio-economic variables, to refine the model's predictive capabilities and support targeted mitigation strategies. ~~Overall, the nonstationary intensity loss functions developed in this paper can serve as a useful tool for drought management.~~

Acknowledgments

This research is supported by the National Natural Science Foundation of China (2023YFF0804900 and 52379033) and the Guangdong Provincial Department of Science and Technology (2019ZT08G090).

CRediT authorship contribution statement

Tongtiegang Zhao: Writing – original draft, Visualization, Software, Methodology, Conceptualization. Zecong Chen: Validation, Resources, Data curation. Yongyong Zhang: Investigation, Formal analysis.

Declaration of competing interest

The authors declare that they have no known competing financial interests or personal relationships that could have appeared to influence the work reported in this paper.

Data Availability Statement

The drought-affected population is available from the Ministry of Water Resources of China (http://www.mwr.gov.cn/sj/tjgb/zgshzhgb/). The CHIRPS precipitation data is available from the Climate Hazards Center at the University of California, Santa Barbara (https://www.chc.ucsb.edu/data/chirps). The SPEI data is available from the Global SPEI database (https://spei.csic.es/database.html). The scPDSI data is available from the the Climatic Research Unit (CRU) at (https://crudata.uea.ac.uk/cru/data/drought/)

带格式的: 超链接, 字体: (中文) 宋体, (中文) 中文(中国)
带格式的: 字体: (默认) Times New Roman
带格式的: 超链接, 字体: (默认) Times New Roman
带格式的: 字体: (默认) Times New Roman
域代码已更改

~~CRU Drought indices~~.

Appendix A : Surface plots and wireframe plots for the nonstationary logistic functions relating the drought-affected population to time and SPEI

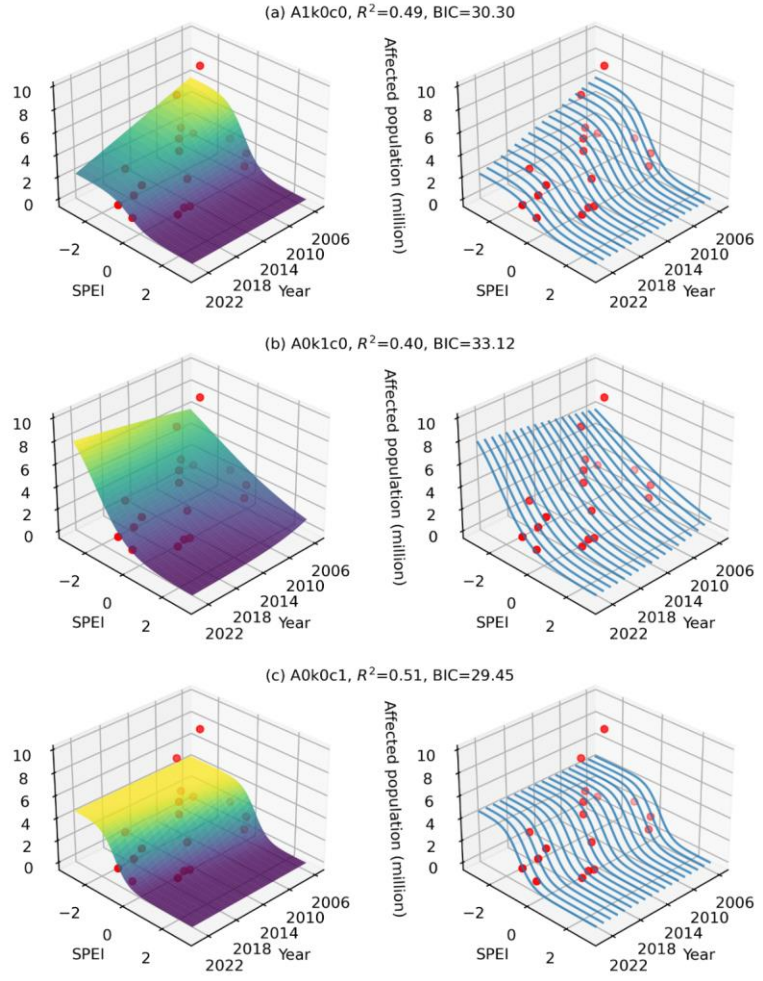

485

Figure A1 Surface plots (left) and wireframe plots (right) for the nonstationary logistic functions (a) A1k0c0, (b) A0k1c0 and (c) A0k0c1 relating the drought-affected population to time and SPEI for Yunnan Province.

带格式的：题注

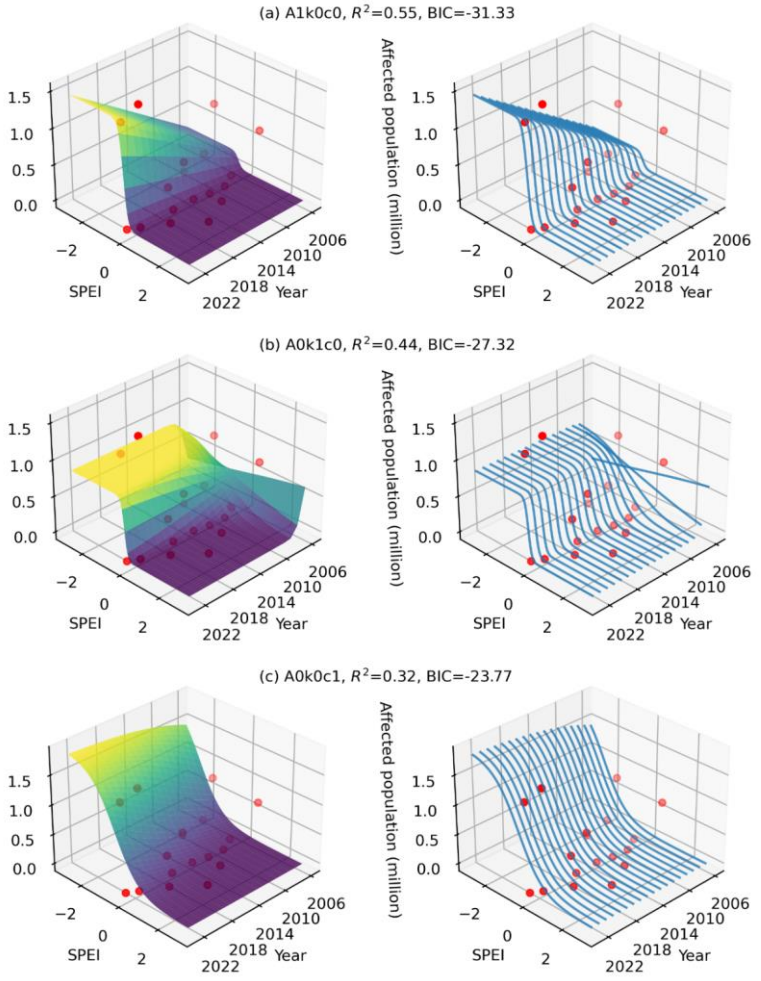

~~Figure A2 Surface plots (left) and wireframe plots (right) for the nonstationary logistic functions (a) A1k0c0, (b) A0k1c0 and (c) A0k0c1 relating the drought-affected population to time and SPEI for Guangdong Province.~~

带格式的: 与下段同页

带格式的: 题注

带格式的: 字体: (中文) +中文正文 (宋体), 非加粗, (中文) 中文(中国)

带格式的: 字体: Times New Roman, 非加粗

Appendix B : Surface plots and wireframe plots for the nonstationary logistic functions relating the drought-affected population to time and scPDSI

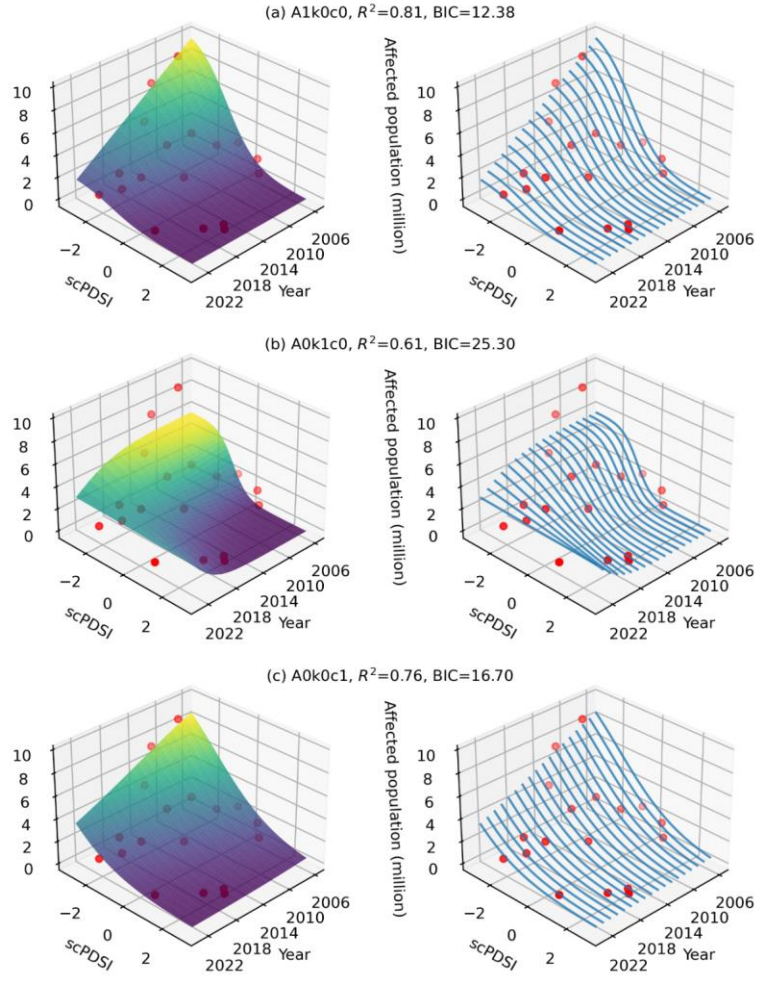

Figure B1 Surface plots (left) and wireframe plots (right) for the nonstationary logistic functions (a) A1k0c0, (b) A0k1c0 and (c) A0k0c1 relating the drought-affected population to time and scPDSI for Yunnan Province.

带格式的: 题注

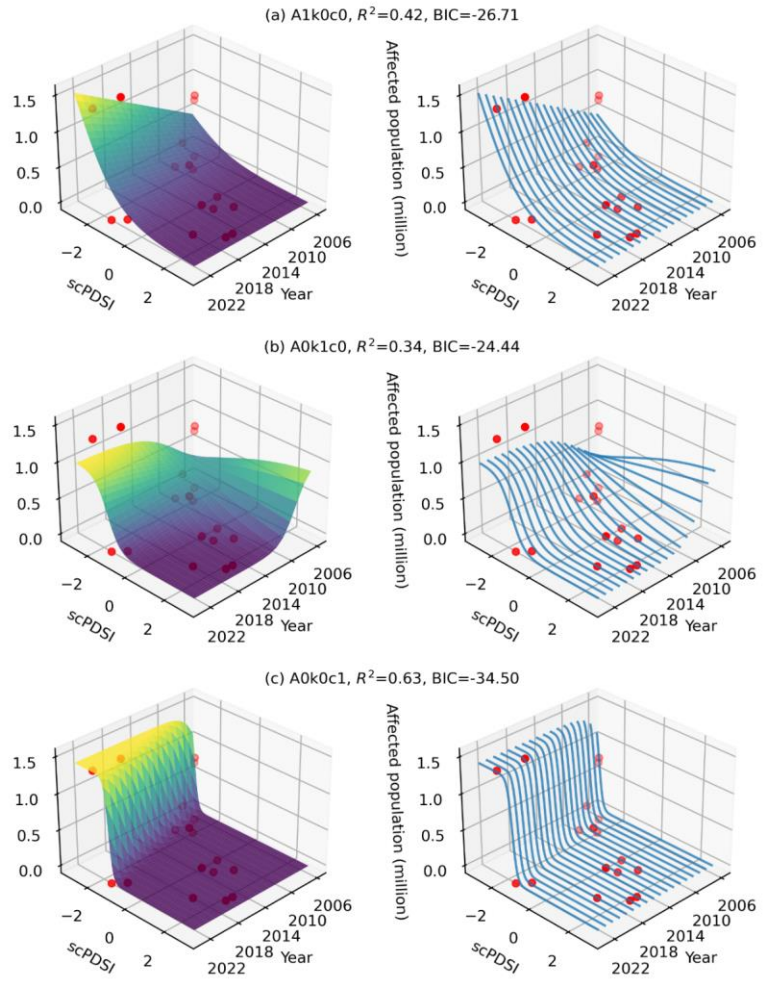

~~**Figure B2 Surface plots (left) and wireframe plots (right) for the nonstationary logistic functions (a) A1k0c0, (b) A0k1c0 and (c) A0k0c1 relating the drought-affected population to time and scPDSI for Guangdong Province.**~~

带格式的: 与下段同页

带格式的: 题注

带格式的: 字体: 小五, 字体颜色: 自动设置

~~**Appendix C : Surface plots and wireframe plots for the nonstationary logistic functions incorporating a quadratic term relating the drought-affected population to time and SPI**~~

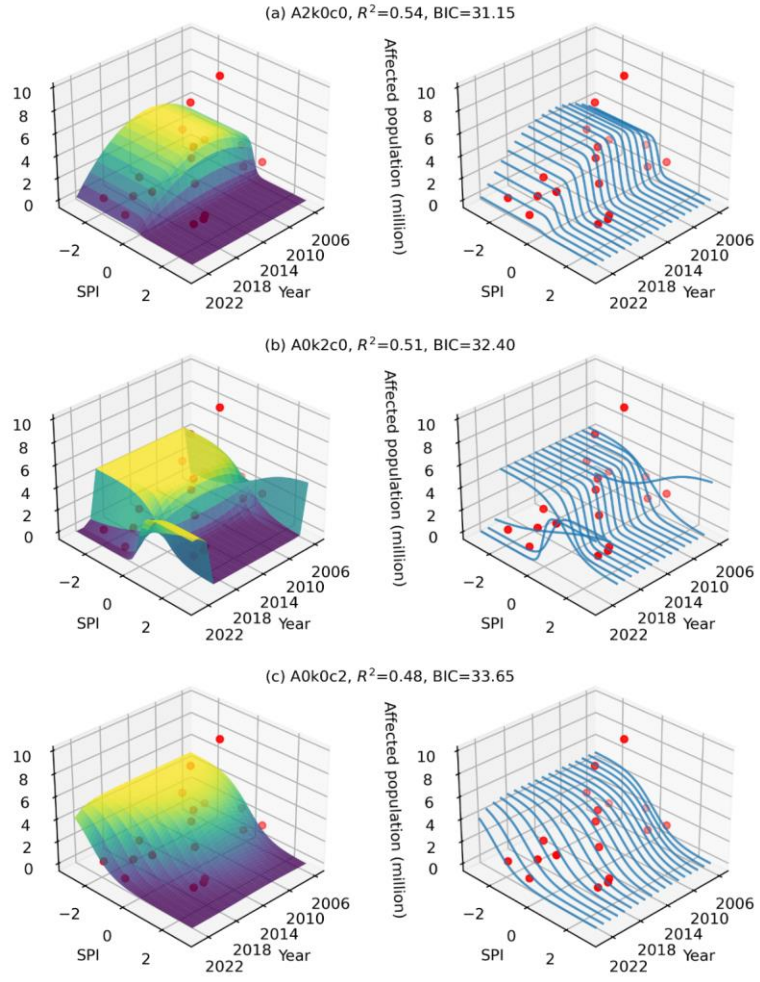

~~**Figure C1 Surface plots (left) and wireframe plots (right) for the nonstationary logistic functions incorporating a quadratic term relating the drought-affected population to time and SPI for Yunnan Province.**~~

带格式的： 与下段同页

带格式的： 题注

带格式的： 字体: 小五, 字体颜色: 自动设置

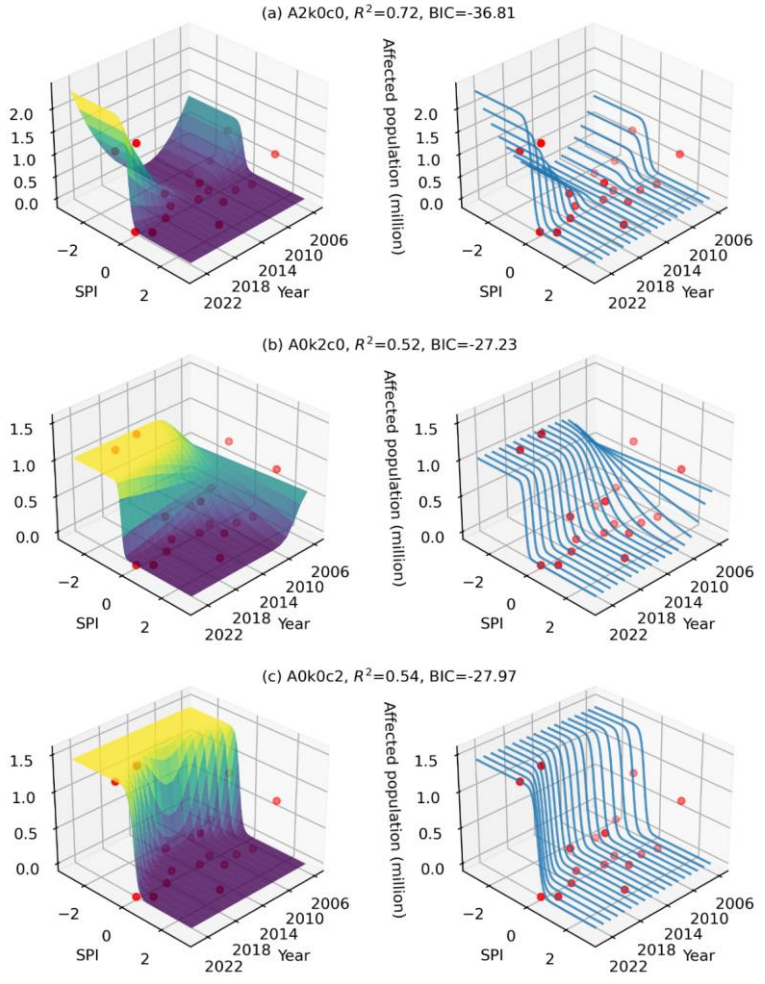

505 ~~**Figure C2 Surface plots (left) and wireframe plots (right) for the nonstationary logistic functions nonstationary logistic functions incorporating a quadratic term relating the drought-affected population to time and SPI for Guangdong Province.**~~

带格式的: 与下段同页

带格式的: 题注

带格式的: 字体: 小五, 字体颜色: 自动设置

Appendix D : 2D heatmaps for for the nonstationary logistic functions (a) A1k0c0, (b) A0k1c0 and (c) A0k0c1 relating the drought-affected population to time and SPI

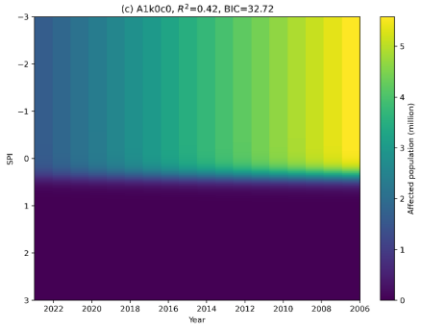

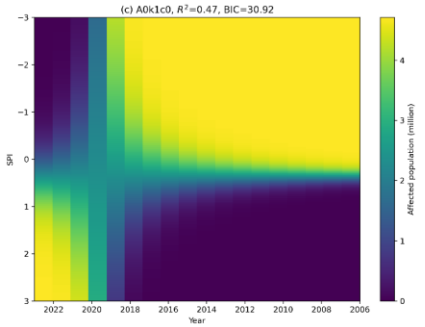

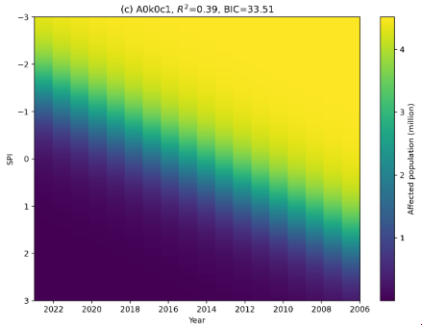

510 **Figure D1 2D heatmaps for for the nonstationary logistic functions (a) A1k0c0, (b) A0k1c0 and (c) A0k0c1 relating the drought-affected population to time and SPI for Yunnan Province.**

带格式的: 与下段同页

带格式的: 题注

带格式的: 字体: 小五, 字体颜色: 自动设置

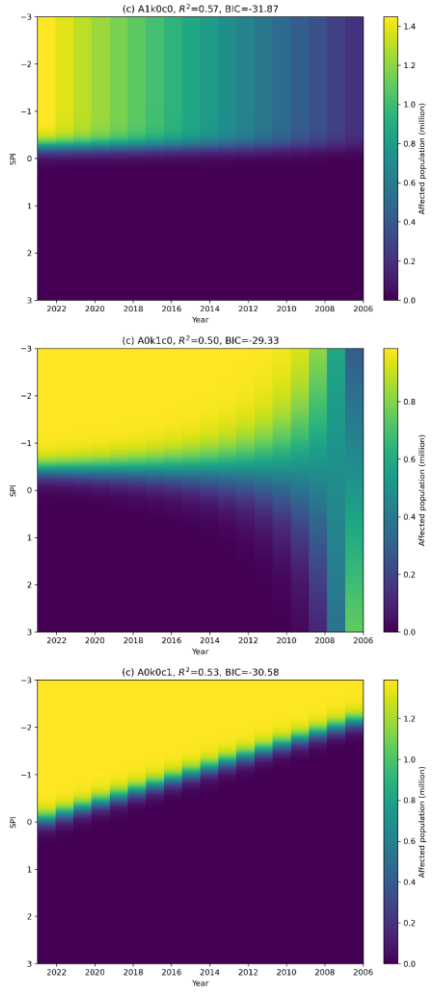

~~**Figure D2 2D heatmaps for for the nonstationary logistic functions (a) A1k0c0, (b) A0k1c0 and (c) A0k0c1 relating the drought affected population to time and SPI for Yunnan Province.**~~

带格式的：与下段同页

带格式的：题注

带格式的：字体: (中文) +中文正文 (宋体), 小五, 字体颜色: 自动设置, (中文) 中文(中国)

References

AghaKouchak, A., Mirchi, A., Madani, K., Di Baldassarre, G., Nazemi, A., Alborzi, A., Anjileli, H., Azarderakhsh, M., Chiang, F., Hassanzadeh, E., Huning, L. S., Mallakpour, I., Martinez, A., Mazdiyasni, O., Moftakhari, H., Norouzi, H., Sadegh, M., Sadeqi, D., Van Loon, A. F., and Wanders, N.: Anthropogenic Drought: Definition, Challenges, and Opportunities, Reviews of Geophysics, 59, e2019RG000683, https://doi.org/10.1029/2019RG000683, 2021.

Apurv, T. and Cai, X.: Regional Drought Risk in the Contiguous United States, Geophysical Research Letters, 48, e2020GL092200, https://doi.org/10.1029/2020GL092200, 2021.

Baez-Villanueva, O. M., Zambrano-Bigiarini, M., Miralles, D. G., Beck, H. E., Siegmund, J. F., Alvarez-Garreton, C., Verbist, K., Garreaud, R., Boisier, J. P., and Galleguillos, M.: On the timescale of drought indices for monitoring streamflow drought considering catchment hydrological regimes, Hydrol. Earth Syst. Sci., 28, 1415–1439, https://doi.org/10.5194/hess-28-1415-2024, 2024.

Barichivich, J., Osborn, T. J., Harris, I., van der Schrier, G., and Jones, P. D.: Monitoring global drought using the self-calibrating palmer drought severity index [in "state of the climate in 2023"], Bulletin of the American Meteorological Society, 105, S70–S71, https://doi.org/10.1175/BAMS-D-24-0116.1, 2024.

Beguería, S., Vicente Serrano, S. M., Reig-Gracia, F., and Latorre García, B.: SPEIbase v.2.10 [dataset]: A comprehensive tool for global drought analysis, https://doi.org/10.13039/501100000780, 2024.

Chen, H. and Zhao, T.: Modeling power loss during blackouts in China using non-stationary generalized extreme value distribution, Energy, 195, 117044, https://doi.org/10.1016/j.energy.2020.117044, 2020.

Chen, M., Ma, J., Hu, Y., Zhou, F., Li, J., and Yan, L.: Is the S-shaped curve a general law? An application to evaluate the damage resulting from water-induced disasters, Nat Hazards, 78, 497–515, https://doi.org/10.1007/s11069-015-1723-9, 2015.

Cheng, L., AghaKouchak, A., Gilleland, E., and Katz, R. W.: Non-stationary extreme value analysis in a changing climate, Climatic Change, 127, 353–369, https://doi.org/10.1007/s10584-014-1254-5, 2014.

Chiang, F., Mazdiyasni, O., and AghaKouchak, A.: Evidence of anthropogenic impacts on global drought frequency, duration, and intensity, Nat Commun, 12, 2754, https://doi.org/10.1038/s41467-021-22314-w, 2021.

Dai, A.: Drought under global warming: a review, WIREs Climate Change, 2, 45–65, https://doi.org/10.1002/wcc.81, 2011.

Entekhabi, D.: Propagation in the Drought Cascade: Observational Analysis Over the Continental US, Water Resources Research, 59, e2022WR032608, https://doi.org/10.1029/2022WR032608, 2023.

Funk, C., Peterson, P., Landsfeld, M., Pedreros, D., Verdin, J., Shukla, S., Husak, G., Rowland, J., Harrison, L., Hoell, A., and Michaelsen, J.: The climate hazards infrared precipitation with stations—a new environmental record for monitoring extremes, Scientific Data, 2, 150066, https://doi.org/10.1038/sdata.2015.66, 2015.

Gao, H., Hrachowitz, M., Wang-Erlandsson, L., Fenicia, F., Xi, Q., Xia, J., Shao, W., Sun, G., and Savenije, H. H. G.: Root zone in the Earth system, Hydrology and Earth System Sciences, 28, 4477–4499, https://doi.org/10.5194/hess-28-4477-2024, 2024a.

Gao, Y., Zhao, T., Tu, T., Tian, Y., Zhang, Y., Liu, Z., Zheng, Y., Chen, X., and Wang, H.: Spatiotemporal links between meteorological and agricultural droughts impacted by tropical cyclones in China, Science of The Total Environment, 912, 169119, https://doi.org/10.1016/j.scitotenv.2023.169119, 2024b.

Gao, Y., Zhao, T., Tu, T., Tian, Y., Zhang, Y., Liu, Z., Zheng, Y., Chen, X., and Wang, H.: Spatiotemporal links between meteorological and agricultural droughts impacted by tropical cyclones in China, Science of The Total Environment, 912, 169119, https://doi.org/10.1016/j.scitotenv.2023.169119, 2024c.

Garrido-Perez, J. M., Vicente-Serrano, S. M., Barriopedro, D., Garc á-Herrera, R., Trigo, R., and Beguer á, S.: Examining the outstanding Euro-Mediterranean drought of 2021–2022 and its historical context, Journal of Hydrology, 630, 130653, https://doi.org/10.1016/j.jhydrol.2024.130653, 2024.

Haile, G. G., Tang, Q., Li, W., Liu, X., and Zhang, X.: Drought: Progress in broadening its understanding, WIREs Water, 7, e1407, https://doi.org/10.1002/wat2.1407, 2020.

Hao, Z. and Singh, V. P.: Drought characterization from a multivariate perspective: A review, Journal of Hydrology, 527, 668–678, https://doi.org/10.1016/j.jhydrol.2015.05.031, 2015.

Hao, Z., Yuan, X., Xia, Y., Hao, F., and Singh, V. P.: An Overview of Drought Monitoring and Prediction Systems at Regional and Global Scales, Bulletin of the American Meteorological Society, 98, 1879–1896, https://doi.org/10.1175/BAMS-D-15-00149.1, 2017.

Hersbach, H., Bell, B., Berrisford, P., Hirahara, S., Horányi, A., Muñoz-Sabater, J., Nicolas, J., Peubey, C., Radu, R., Schepers, D., Simmons, A., Soci, C., Abdalla, S., Abellan, X., Balsamo, G., Bechtold, P., Biavati, G., Bidlot, J., Bonavita, M., De Chiara, G., Dahlgren, P., Dee, D., Diamantakis, M., Dragani, R., Flemming, J., Forbes, R., Fuentes, M., Geer, A., Haimberger, L., Healy, S., Hogan, R. J., Hólm, E., Janisková, M., Keeley, S., Laloyaux, P., Lopez, P., Lupu, C., Radnoti, G., De Rosnay, P., Rozum, I., Vamborg, F., Villaume, S., and Thépaut, J.: The ERA5 global reanalysis, Quart J Royal Meteoro Soc, 146, 1999–2049, https://doi.org/10.1002/qj.3803, 2020.

Hoerling, M., Eischeid, J., Kumar, A., Leung, R., Mariotti, A., Mo, K., Schubert, S., and Seager, R.: Causes and Predictability of the 2012 Great Plains Drought, Bulletin of the American Meteorological Society, 95, 269–282, https://doi.org/10.1175/BAMS-D-13-00055.1, 2014.

Hou, W., Chen, Z.-Q., Zuo, D.-D., and Feng, G.: Drought loss assessment model for southwest China based on a hyperbolic tangent function, International Journal of Disaster Risk Reduction, 33, 477–484, https://doi.org/10.1016/j.ijdrr.2018.01.017, 2019.

Jonkman, S. N., Vrijling, J. K., and Vrouwenvelder, A. C. W. M.: Methods for the estimation of loss of life due to floods: a literature review and a proposal for a new method, Nat Hazards, 46, 353–389, https://doi.org/10.1007/s11069-008-9227-5, 2008.

Kucharavy, D. and De Guio, R.: Application of S-shaped curves, Procedia Engineering, 9, 559–572, https://doi.org/10.1016/j.proeng.2011.03.142, 2011.

Liu, R., Yin, J., Slater, L., Kang, S., Yang, Y., Liu, P., Guo, J., Gu, X., Zhang, X., and Volchak, A.: Machine-learning-constrained projection of bivariate hydrological drought magnitudes and socioeconomic risks over China, Hydrol. Earth Syst. Sci., 28, 3305–3326, https://doi.org/10.5194/hess-28-3305-2024, 2024.

Long, D., Yang, W., Scanlon, B. R., Zhao, J., Liu, D., Burek, P., Pan, Y., You, L., and Wada, Y.: South-to-North Water Diversion stabilizing Beijing's groundwater levels, Nat Commun, 11, 3665, https://doi.org/10.1038/s41467-020-17428-6, 2020.

Lü, J., Ju, J., Ren, J., and Gan, W.: The influence of the Madden-Julian Oscillation activity anomalies on Yunnan's extreme drought of 2009–2010, Sci. China Earth Sci., 55, 98–112, https://doi.org/10.1007/s11430-011-4348-1, 2012.

Ma, M., Qu, Y., Lyu, J., Zhang, X., Su, Z., Gao, H., Yang, X., Chen, X., Jiang, T., Zhang, J., Shen, M., and Wang, Z.: The 2022 extreme drought in the Yangtze River Basin: Characteristics, causes and response strategies, River, 1, 162–171, https://doi.org/10.1002/rvr2.23, 2022.

Mishra, A. K. and Singh, V. P.: A review of drought concepts, Journal of Hydrology, 391, 202–216, https://doi.org/10.1016/j.jhydrol.2010.07.012, 2010.

Montanari, A., Nguyen, H., Rubinetti, S., Ceola, S., Galelli, S., Rubino, A., and Zanchettin, D.: Why the 2022 Po River drought is the worst in the past two centuries, Sci. Adv., 9, eadg8304, https://doi.org/10.1126/sciadv.adg8304, 2023.

Neath, A. A. and Cavanaugh, J. E.: The Bayesian information criterion: background, derivation, and applications, WIREs Computational Stats, 4, 199–203, https://doi.org/10.1002/wics.199, 2012.

Pradhan, R. K., Markonis, Y., Vargas Godoy, M. R., Villalba-Pradas, A., Andreadis, K. M., Nikolopoulos, E. I., Papalexiou, S. M., Rahim, A., Tapiador, F. J., and Hanel, M.: Review of GPM IMERG performance: A global perspective, Remote Sensing of Environment, 268, 112754, https://doi.org/10.1016/j.rse.2021.112754, 2022.

Qiu, M., Ratledge, N., Azevedo, I. M. L., Diffenbaugh, N. S., and Burke, M.: Drought impacts on the electricity system, emissions, and air quality in the western United States, Proc. Natl. Acad. Sci. U.S.A., 120, e2300395120, https://doi.org/10.1073/pnas.2300395120, 2023.

van der Schrier, G., Barichivich, J., Briffa, K. R., and Jones, P. D.: A scPDSI-based global data set of dry and wet spells for 1901–2009, Journal of Geophysical Research: Atmospheres, 118, 4025–4048, https://doi.org/10.1002/jgrd.50355, 2013.

Shao, Q., Liu, X., and Zhao, W.: An alternative method for analyzing dimensional interactions of urban carrying capacity: Case study of Guangdong-Hong Kong-Macao Greater Bay Area, Journal of Environmental Management, 273, 111064, https://doi.org/10.1016/j.jenvman.2020.111064, 2020.

Shi, W., Huang, S., Liu, D., Huang, Q., Han, Z., Leng, G., Wang, H., Liang, H., Li, P., and Wei, X.: Drought-flood abrupt alternation dynamics and their potential driving forces in a changing environment, Journal of Hydrology, 597, 126179, https://doi.org/10.1016/j.jhydrol.2021.126179, 2021.

Su, B., Huang, J., Fischer, T., Wang, Y., Kundzewicz, Z. W., Zhai, J., Sun, H., Wang, A., Zeng, X., Wang, G., Tao, H., Gemmer, M., Li, X., and Jiang, T.: Drought losses in China might double between the 1.5 ℃ and 2.0 ℃ warming, Proc. Natl. Acad. Sci. U.S.A., 115, 10600–10605, https://doi.org/10.1073/pnas.1802129115, 2018.

Sun, S., Zhou, X., Liu, H., Jiang, Y., Zhou, H., Zhang, C., and Fu, G.: Unraveling the effect of inter-basin water transfer on reducing water scarcity and its inequality in China, Water Research, 194, 116931, https://doi.org/10.1016/j.watres.2021.116931, 2021.

Todisco, F., Mannocchi, F., and Vergni, L.: Severity–duration–frequency curves in the mitigation of drought impact: an agricultural case study, Nat Hazards, 65, 1863–1881, https://doi.org/10.1007/s11069-012-0446-4, 2013.

Tsoularis, A. and Wallace, J.: Analysis of logistic growth models, Mathematical Biosciences, 179, 21–55, https://doi.org/10.1016/S0025-5564(02)00096-2, 2002.

Van Dijk, A. I. J. M., Beck, H. E., Crosbie, R. S., De Jeu, R. A. M., Liu, Y. Y., Podger, G. M., Timbal, B., and Viney, N. R.: The Millennium Drought in southeast Australia (2001–2009): Natural and human causes and implications for water resources, ecosystems, economy, and society, Water Resources Research, 49, 1040–1057, https://doi.org/10.1002/wrcr.20123, 2013.

Virtanen, P., Gommers, R., Oliphant, T. E., Haberland, M., Reddy, T., Cournapeau, D., Burovski, E., Peterson, P., Weckesser, W., Bright, J., Van Der Walt, S. J., Brett, M., Wilson, J., Millman, K. J., Mayorov, N., Nelson, A. R. J., Jones, E., Kern, R., Larson, E., Carey, C. J., Polat, İ., Feng, Y., Moore, E. W., VanderPlas, J., Laxalde, D., Perktold, J., Cimrman, R., Henriksen, I., Quintero, E. A., Harris, C. R., Archibald, A. M., Ribeiro, A. H., Pedregosa, F., Van Mulbregt, P., SciPy 1.0 Contributors, Vijaykumar, A., Bardelli, A. P., Rothberg, A., Hilboll, A., Kloeckner, A., Scopatz, A., Lee, A., Rokem, A., Woods, C. N., Fulton, C., Masson, C., Häggström, C., Fitzgerald, C., Nicholson, D. A., Hagen, D. R., Pasechnik, D. V., Olivetti, E., Martin, E., Wieser, E., Silva, F., Lenders, F., Wilhelm, F., Young, G., Price, G. A., Ingold, G.-L., Allen, G. E., Lee, G. R., Audren, H., Probst, I., Dietrich, J. P., Silterra, J., Webber, J. T., Slavič, J., Nothman, J., Buchner, J., Kulick, J., Schönberger, J. L., De Miranda Cardoso, J. V., Reimer, J., Harrington, J., Rodríguez, J. L. C., Nunez-Iglesias, J., Kuczynski, J., Tritz, K., Thoma, M., Newville, M., Kümmerer, M., Bolingbroke, M., Tartre, M., Pak, M., Smith, N. J., Nowaczyk, N., Shebanov, N., Pavlyk, O., Brodtkorb, P. A., Lee, P., McGibbon, R. T., Feldbauer, R., Lewis, S., Tygier, S., Sievert, S., Vigna, S., Peterson, S., More, S., et al.: SciPy 1.0: fundamental algorithms for scientific computing in Python, Nat Methods, 17, 261–272, https://doi.org/10.1038/s41592-019-0686-2, 2020.

Wan, L., Zhou, J., Guo, H., Cui, M., and Liu, Y.: Trend of water resource amount, drought frequency, and agricultural exposure to water stresses in the karst regions of South China, Natural Hazards, 80, 23–42, https://doi.org/10.1007/s11069-015-1954-9, 2016.

Wang, F., Lai, H., Li, Y., Feng, K., Tian, Q., Zhang, Z., Di, D., and Yang, H.: Terrestrial ecological drought dynamics and its response to atmospheric circulation factors in the North China Plain, Atmospheric Research, 294, 106944, https://doi.org/10.1016/j.atmosres.2023.106944, 2023a.

Wang, Y., Wang, S., Chen, Y., Wang, F., Liu, Y., and Zhao, W.: Anthropogenic drought in the Yellow River basin: Multifaceted and weakening connections between meteorological and hydrological droughts, Journal of Hydrology, 619, 129273, https://doi.org/10.1016/j.jhydrol.2023.129273, 2023b.

Wells, N., Goddard, S., and Hayes, M. J.: A self-calibrating palmer drought severity index, Journal of Climate, 17, 2335–2351, https://doi.org/10.1175/1520-0442(2004)017<2335:ASPDSI>2.0.CO;2, 2004.

Weng, P., Tian, Y., Zhou, H., Zheng, Y., and Jiang, Y.: Saltwater intrusion early warning in Pearl river Delta based on the temporal clustering method, Journal of Environmental Management, 349, 119443, https://doi.org/10.1016/j.jenvman.2023.119443, 2024.

West, H., Quinn, N., and Horswell, M.: Remote sensing for drought monitoring & impact assessment: Progress, past challenges and future opportunities, Remote Sensing of Environment, 232, 111291, https://doi.org/10.1016/j.rse.2019.111291, 2019.

Wu, Z., Li, J., He, J., and Jiang, Z.: Occurrence of droughts and floods during the normal summer monsoons in the mid- and lower reaches of the Yangtze River, Geophysical Research Letters, 33, https://doi.org/10.1029/2005GL024487, 2006.

Xiong, L., Du, T., Xu, C.-Y., Guo, S., Jiang, C., and Gippel, C. J.: Non-Stationary Annual Maximum Flood Frequency Analysis Using the Norming Constants Method to Consider Non-Stationarity in the Annual Daily Flow Series, Water Resour Manage, 29, 3615–3633, https://doi.org/10.1007/s11269-015-1019-6, 2015.

Yang, X., Wu, F., Yuan, S., Ren, L., Sheffield, J., Fang, X., Jiang, S., and Liu, Y.: Quantifying the Impact of Human Activities on Hydrological Drought and Drought Propagation in China Using the PCR-GLOBWB v2.0 Model, Water Resources Research, 60, e2023WR035443, https://doi.org/10.1029/2023WR035443, 2024.

Ye, L., Hanson, L. S., Ding, P., Wang, D., and Vogel, R. M.: The probability distribution of daily precipitation at the point and catchment scales in the United States, Hydrol. Earth Syst. Sci., 22, 6519–6531, https://doi.org/10.5194/hess-22-6519-2018, 2018.

Yin, J., Slater, L., Gu, L., Liao, Z., Guo, S., and Gentine, P.: Global Increases in Lethal Compound Heat Stress: Hydrological Drought Hazards Under Climate Change, Geophysical Research Letters, 49, e2022GL100880, https://doi.org/10.1029/2022GL100880, 2022.

Yuan, X., Wang, Y., Ji, P., Wu, P., Sheffield, J., and Otkin, J. A.: A global transition to flash droughts under climate change, Science, 380, 187–191, https://doi.org/10.1126/science.abn6301, 2023.

Zhang, L., Yuan, F., and He, X.: Probabilistic Assessment of Global Drought Recovery and Its Response to Precipitation Changes, Geophysical Research Letters, 51, e2023GL106067, https://doi.org/10.1029/2023GL106067, 2024.

Zhang, X., Hao, Z., Singh, V. P., Zhang, Y., Feng, S., Xu, Y., and Hao, F.: Drought propagation under global warming: Characteristics, approaches, processes, and controlling factors, Science of The Total Environment, 838, 156021, https://doi.org/10.1016/j.scitotenv.2022.156021, 2022.

Zhang, Y., Keenan, T. F., and Zhou, S.: Exacerbated drought impacts on global ecosystems due to structural overshoot, Nat Ecol Evol, 5, 1490–1498, https://doi.org/10.1038/s41559-021-01551-8, 2021.

Zhao, T., Chen, Z., Tian, Y., Zhang, B., Li, Y., and Chen, X.: A decomposition approach to evaluating the local performance of global streamflow reanalysis, Hydrology and Earth System Sciences, 28, 3597–3611, https://doi.org/10.5194/hess-28-3597-2024, 2024a.

Zhao, T., Li, X., Li, Y., Zhang, B., and Zhang, Y.: Concurrent droughts across Major River Basins of the World modulated by El Niño–Southern Oscillation, Journal of Hydrology, 644, 132112, https://doi.org/10.1016/j.jhydrol.2024.132112, 2024b.